New Phytologist

Research

MTA1-mediated RNA m^{6}A modification regulates autophagy and is required for infection of the rice blast fungus

Zhiyong Ren[1]*, Bozeng Tang[2]*, Junjie Xing[3], Caiyun Liu[1], Xuan Cai[1], Ahmed Hendy[1], Muhammad Kamran[1], Hao Liu[1], Lu Zheng[1], Junbing Huang[1] and Xiao-Lin Chen[1,3]

[1]State Key Laboratory of Agricultural Microbiology, Provincial Key Laboratory of Plant Pathology of Hubei Province, College of Plant Science and Technology, Huazhong Agricultural University, Wuhan 430070, China; [2]The Sainsbury Laboratory, University of East Anglia, Norwich Research Park, NR4 7UH, Norwich, UK; [3]State Key Laboratory of Hybrid Rice, Hunan Hybrid Rice Research Center, Changsha 410125, China

Author for correspondence:
Xiao-Lin Chen
Email: chenxiaolin@mail.hzau.edu.cn

Received: *17 October 2021*
Accepted: *8 March 2022*

New Phytologist (2022) **235:** 247–262
doi: 10.1111/nph.18117

Key words: appressorium maturation, autophagy, fungal infection, m^{6}A methylation, m^{6}A methyltransferase, *Magnaporthe oryzae*.

Summary

- In eukaryotes, N^6-methyladenosine (m^{6}A) is abundant on mRNA, and plays key roles in the regulation of RNA function. However, the roles and regulatory mechanisms of m^{6}A in phytopathogenic fungi are still largely unknown.
- Combined with biochemical analysis, MeRIP-seq and RNA-seq methods, as well as biological analysis, we showed that *Magnaporthe oryzae MTA1* gene is an orthologue of human *METTL4*, which is involved in m^{6}A modification and plays a critical role in autophagy for fungal infection.
- The Δ*mta1* mutant showed reduced virulence due to blockage of appressorial penetration and invasive growth. Moreover, the autophagy process was severely disordered in the mutant. MeRIP-seq identified 659 hypomethylated m^{6}A peaks covering 595 mRNAs in Δ*mta1* appressoria, 114 m^{6}A peaks was negatively related to mRNA abundance, including several *ATG* gene transcripts. Typically, the mRNA abundance of *MoATG8* was also increased in the single m^{6}A site mutant Δ*atg8*/*MoATG8*^{A982C}, leading to an autophagy disorder.
- Our findings reveal the functional importance of the m^{6}A methylation in infection of *M. oryzae* and provide novel insight into the regulatory mechanisms of plant pathogenic fungi.

Introduction

More than 100 chemical modifications have been found in eukaryotic RNA, and these modifications can act on RNA processing or metabolism (Motorin & Helm, 2011). N^6 methyladenosine (m^{6}A), the methyl substitution of the sixth nitrogen atom (N^6) on RNA adenosine, is the most common and abundant RNA modification in eukaryotic mRNA (Fu *et al.*, 2014). The m^{6}A modification is a reversible chemical modification that is regulated by methyltransferases as writers, demethyltransferases as erasers and m^{6}A recognising proteins as readers (Fu *et al.*, 2014; He & He, 2021).

The m^{6}A writer is found to be a methyltransferase complex in different organisms including human, mouse, fruit fly and zebrafish, and is commonly composed of METTL3, METTL14 and other protein subunits such as WTAP or Zc3h13 (Liu *et al.*, 2014; Ping *et al.*, 2014; Schwartz *et al.*, 2014; Wang *et al.*, 2014; Wen *et al.*, 2018; Yue *et al.*, 2018). METTL3 is the first identified m^{6}A writer that plays a central catalytic role on methyl groups and transfers them from the *S*-adenosylmethionine (SAM) moiety to adenine, whereas METTL14 promotes substrate binding and WTAP affects m6A methyltransferase activity and nuclear localisation (Wang *et al.*, 2016). This complex mainly targets the mRNAs in the region near the stop codon. Some other methyltransferases are also found to catalyse m^{6}A, including METTL16, METTL5, ZCCHC4 and METTL4 (Pendleton *et al.*, 2017; Warda *et al.*, 2017; Ma *et al.*, 2019; van Tran *et al.*, 2019; Gu *et al.*, 2020). METTL16 is found to methylate mRNA of MAT2A at the 3′ UTR region (Pendleton *et al.*, 2017). METTL5 and ZCCHC4 can also function as the m^{6}A writers to catalyse 18S rRNA and 28S rRNA, respectively (van Tran *et al.*, 2019). Recently, METTL4 was also found to be an m^{6}A writer that methylates U2 small nuclear RNA (snRNA) at internal positions in *Drosophila melanogaster* (Gu *et al.*, 2020). YTH domain proteins are usually the m6A readers, while fat mass and obesity-associated (FTO) protein and alkylated DNA repair protein AlkB homologue 5 (ALKBH5) are the erasers (Jia *et al.*, 2011; Zheng *et al.*, 2013; Liu *et al.*, 2015).

RNA m^{6}A modification has been discovered to play an important role in RNA metabolism, including mRNA stability, translation efficiency, RNA splicing, nuclear export and RNA structure (Liu *et al.*, 2015; Meyer *et al.*, 2015; Wang *et al.*, 2015; Lin *et al.*, 2016). In HeLa cells, m^{6}A mainly targets transcripts for degradation and delivery to P bodies (Yue *et al.*, 2018). In embryonic stem cells, m^{6}A modification blocks the antigen R (HuR) binding to particular mRNAs in the 3′ region and preventing their degradation (Visvanathan *et al.*, 2018). Therefore, m^{6}A usually negatively correlates with the half-life of mRNA.

*These authors contributed equally to this work.

Human circadian rhythms, stem cell pluripotency, and cancer stem cell proliferation have all been linked to m6A (Fustin *et al.*, 2013; Batista *et al.*, 2014; Geula *et al.*, 2015), in addition to these functions, m^6A controls sex determination in *D. melanogaster* (Lence *et al.*, 2016; Kan *et al.*, 2017). The m^6A also plays a key role in female oocyte maturation and cerebellar development in mammals, and maternal-to-zygotic transition in zebrafish (Aguilo *et al.*, 2015; Ivanova *et al.*, 2017; Zhao *et al.*, 2017). In plants, m^6A is important for normal trichome morphology, floral transition, timing and execution (Shen *et al.*, 2016; Arribas-Hernández *et al.*, 2018; Wei *et al.*, 2018). In yeast *Saccharomyces cerevisiae*, the m^6A writer Ime4, a homologue of human METTL3, regulates triacylglycerol (TAG) metabolism, vacuolar morphology and mitochondrial morphology in haploid cells (Clancy *et al.*, 2002; Yadav *et al.*, 2017, 2018). However, the function of m^6A is largely unknown in filamentous fungi.

Autophagy is an evolutionarily conserved degradation pathway that starts with the formation of autophagosomes and finally fuses with lysosome or vacuole to degrade organelles and proteins for recycling (Bento *et al.*, 2016; Yu *et al.*, 2018). The autophagy process is finely regulated by a series of autophagy-related proteins (ATG), among which Atg8 is the most critical one that induces autophagy and subsequent vesicular compartmentation (Ohsumi, 2014; Shibutani *et al.*, 2015). The newly synthesised Atg8 precursor is activated by cleaving the carboxyl-terminal sequence. Then, the E1 and E2 enzymes (Atg7 and Atg3) regulate the formation of the Atg8–phosphatidylethanolamine (PE) conjugate for ubiquitination reaction (Bento *et al.*, 2016; Yu *et al.*, 2018). To date, regulation of the autophagy process has mainly focused on the transactivation of autophagy-related genes and the posttranslational modification (PTM) (Wani *et al.*, 2015; Füllgrabe *et al.*, 2016). For example, acetylation of ATG proteins has been proved to be important for regulation of autophagy (He *et al.*, 2018).

In the past decade, studies have shown that autophagy is crucial for the development and infection of plant pathogenic fungi, especially in the rice blast fungus *Magnaporthe oryzae* (Veneault-Fourrey *et al.*, 2006; Liu *et al.*, 2012; Zhu *et al.*, 2019). The appressorium maturation process requires the quick utilisation of the conidial storage to facilitate appressorial turgor generation for host penetration (Wilson & Talbot, 2009). This process is accompanied by autophagic cell death, which is essential for fungal infection (Kershaw & Talbot, 2009). Autophagy-related genes of *M. oryzae* can regulate conidial cell death, appressorium maturation and penetration, supporting the key role of autophagy at the appressorium formation stage (Deng *et al.*, 2009; Kershaw & Talbot, 2009; Deng & Naqvi, 2010). The appressorium development in *M. oryzae* is controlled by cell cycle progression, which is regulated by autophagy (He *et al.*, 2012). By modulating the cell cycle, glucose-ABL1-TOR signalling is found to control terminal appressorial cell differentiation (Marroquin-Guzman *et al.*, 2015, 2017). Recent studies have suggested that MoSnt2-mediated deacetylation of histone H3 is also involved in MoTor-dependent autophagy (He *et al.*, 2018). Another study revealed that acetylation of MoAtg3 and MoAtg9 by MoHat1 is important for appressorium-mediated infection (Yin *et al.*, 2019). However, the regulatory mechanism of appressorial autophagy remains largely unknown.

In this study, we found that MTA1-mediated m^6A modification of the transcripts of ATG genes and serves as a novel regulatory mechanism of appressorial autophagy. Our work demonstrates the important role of mRNA m^6A modification in appressorium-mediated infection of *M. oryzae*.

Materials and Methods

Gene knockout and complementation

All the strains used in this study are listed in Supporting Information Table S1, and *M. oryzae* strain P131 was used as the wild-type strain. *MTA1* and *ATG8* genes were deleted using a split-PCR-mediated gene deletion strategy (Goswami, 2012). Information on all strains and vectors can be found in Tables S1, S2.

Observation of autophagy and western blot

The hyphae of wild-type (WT)/green fluorescent protein (GFP):ATG8 and Δ*mta1*/GFP:ATG8 were cultured in a liquid CM medium at 28°C and 160 rpm for 48 h. Then the hyphae were transferred to MM-N medium and induced for 5 h. The autophagosome formation was observed through GFP:ATG8 fluorescence, and the number of puncta reflects the activity of autophagy, which was quantified using ImageJ software. Under a laser confocal microscope TCS SP8 (Leica Microsystems, Mannheim, Germany) equipped with a pulsed white light laser (470–670 nm), the GFP:ATG8 micrographs were photographed using a 488 nm excitation laser and emission at 510–540 nm with a ×63 oil-immersion objective (1.3 NA). For 3D interpretations of z-stacks, the images were acquired with 8–12 slices at a distance of 0.2-μm separation (Z step size). The spore suspensions of different strains were inoculated on the hydrophobic surface, and then the subcellular localisation of ATG8 was observed at 0, 2 and 4 h. To detect the effects of *MTA1* knockout and m^6A modification on autophagy, the mycelia of different strains were cultured in liquid CM medium for 48 h and then transferred to MM-N medium for 2 or 5 h. Total protein was extracted using an IP cell lysate (Biyuntian, Beijing, China) and separated using SDS-PAGE for western blotting with an anti-GFP primary antibody (1 : 5000; Sigma).

Detection of methylation level of m^6A RNA and ^6mA DNA

The methylation level of m^6A RNA was detected using the EpiQuik™ m^6A RNA methylation quantitative kit (Epigentek, Farmingdale, NY, USA). Here, 200 ng of total input RNA was incorporated into each well of the 8-well plate. The capture antibody, detection antibody and enhancer antibody are sequentially added. Then the developer solution is added, and the colour development of the kit solution is finally stopped. The relative value of methylation of m^6A RNA was then calculated. Similarly, the total DNA samples were used to detect ^6mA DNA methylation level with the same methylation quantitative kit (Epigentek).

Dot blot assay

Total RNA from the WT and the Δ*mta1* mutant were extracted and spotted onto Hybond™-N+ membrane. The membrane was dried at 37°C for 30 min and crosslinked using an HL-2000 HybriLinker for 5 min. After 1 h block in 5% milk phosphate-buffered saline Tween (PBST), the membrane was incubated with an m^{6}A antibody (EpiGentek). The membrane was washed using PBST and incubated with the secondary antibody for 1 h at room temperature. Finally, the ECL detection system (Amersham Bioscience, Piscataway, NJ, USA) was used for visualisation, and then ImageJ software was used for quantification. Briefly, the photographed images were opened in the ImageJ software, and converted to greyscale by setting the toolbar: Image > Type > 8-bit. Select one dot region and define it as a region of interest (ROI), then go to Analyze > Gels > Plot Lanes to draw a profile plot for each ROI. The profile plot represents the density of the ROI, which can be used to calculate the relative density.

m^{6}A-seq analysis

Appressoria formed by *M. oryzae* conidial suspension of wild-type and the Δ*mta1* mutant on the hydrophobic surface at 12 h post-inoculation (hpi) were harvested. For each strain, two biological replicates were used for assessment. Total RNA was extracted using TRIzol reagent (Invitrogen) following the manufacturer's procedure. Here, *c.* 200 μg of total RNA was subjected to isolate poly(A) mRNA with a poly-T oligo attached magnetic beads (Invitrogen). Following purification, the poly(A) mRNA fractions were fragmented into *c.* 100-nt-long oligonucleotides. Then the cleaved RNA fragments were subjected to incubation for 2 h at 4°C with m^{6}A-specific antibody (No. 202 003; Synaptic Systems, Goettingen, Germany). The mixture was then incubated with protein-A beads and eluted with elution buffer. Eluted m^{6}A-containing fragments (IP) and untreated input control fragments were converted to the final cDNA library. Sequencing was performed on an Illumina Novaseq™ 6000 platform at Lc-Bio Biotech Ltd (Hangzhou, China) following the vendor's recommended protocol. The peak calling was executed by running the function *exomepeak* in R with default settings, and comparing the IP and Input reads. The minimum number of reads was 30. The cut-off to define peak is filtered by fold change > 2 (IP/Input), and false discovery rate (FDR) is < 0.05. More details about settings could be checked in https://bioconductor.riken.jp/packages/3.1/bioc/manuals/exomePeak/man/exomePeak.pdf. The peak calling provides a region that is potentially enriched in m^{6}A modified transcripts. The particular modified sites could only be predicted further using Sramp (http://www.cuilab.cn/sramp).

RNA-seq analysis

Total RNA was isolated from appressorium samples of wild-type and the Δ*mta1* mutant collected from hydrophobic surfaces at 12 hpi. For each strain, three biological replicates were used for assessment. After the quality control (QC) procedures, mRNA from eukaryotic organisms was enriched using oligo(dT) beads. The extracted mRNA was broken randomly into short fragments by the fragmentation buffer. The fragmented mRNA was used as a template to synthesise a strand of cDNA and then perform two-strand cDNA synthesis. After purification with AMPure XP beads, the library was used for sequencing using the Illumina Novase 6000 system. Differentially expressed genes were determined using DESeq2 and a threshold of $\log_2|FC|$ and adjusted *P*-values ($P < 0.05$). for enrichment analysis, ClusterProfiler was used to perform Kyoto Encyclopedia of Genes and Genomes (KEGG) metabolic pathways enrichment analysis.

Quantitative real-time PCR and methylated RNA immunoprecipitation-qPCR

To detect the dynamic expression of related genes in *M. oryzae* and host genes, total RNA was extracted from the strain or rice samples using RNAiso plus (Takara, Beijing, China), and then cDNA was produced using PrimeScript™ II Reverse Transcriptase (Takara, Dalian, China) and random hexamers. Using the SYBR Green PCR Master Mix (Takara), qRT-PCR was performed on the ABI 7500 real-time PCR system (Applied Biosystems, Foster City, CA, USA). For MeRIP-qPCR, the appressorium samples of the wild-type and Δ*mta1* mutant were used for the IP assays. The m^{6}A-IP experiment was performed in the same way as the m^{6}A-seq analysis, and the subsequent MeRIP-qPCR experiment was similar to qRT-PCR using IP assay products as the template. For strand-specific qRT-PCR, total mRNA was used to perform reverse transcription using specific primer priming for the intron region of ATG8 (intron of actin gene *ACT1* was used as a control). Subsequently, qRT-PCR was performed to detect the ATG8 intron level, which could demonstrate the transcription rate (pre-mRNA).

Results

Identification of m^{6}A methyltransferase in *M. oryzae*

To investigate m^{6}A modification in *M. oryzae*, we searched for the homologous protein of N^6 adenosine methyltransferase catalytic subunit METTL3 and noncatalytic subunit METTL14 in the *M. oryzae* genome database. Although homologous proteins of human METTL3 or METTL14 could be found in basidiomycete fungi such as *Ustilago maydis* and *Puccinia graminis*, these were not found in ascomycete fungi including *M. oryzae* (Fig. 1a). Interestingly, using human METTL4, another N^6-adenine-specific methyltransferase, as a query, we identified a homologous protein MGG_01492 in *M. oryzae*, named MT-A70 domain protein 1 (MTA1). This protein contains 376 amino acids with an MT-A70 domain (Fig. 1b), which is commonly contained in the *S*-adenosylmethionine-binding subunit of human mRNA N^6-adenosine-methyltransferase (MTase) and specifically methylates adenines in pre-mRNAs. Phylogenetic tree analysis confirmed that *M. oryzae* MTA1 is indeed closer to human and mouse METTL4, but far from human METTL3, METTL14 or *S. cerevisiae* IME4 (Fig. 1c).

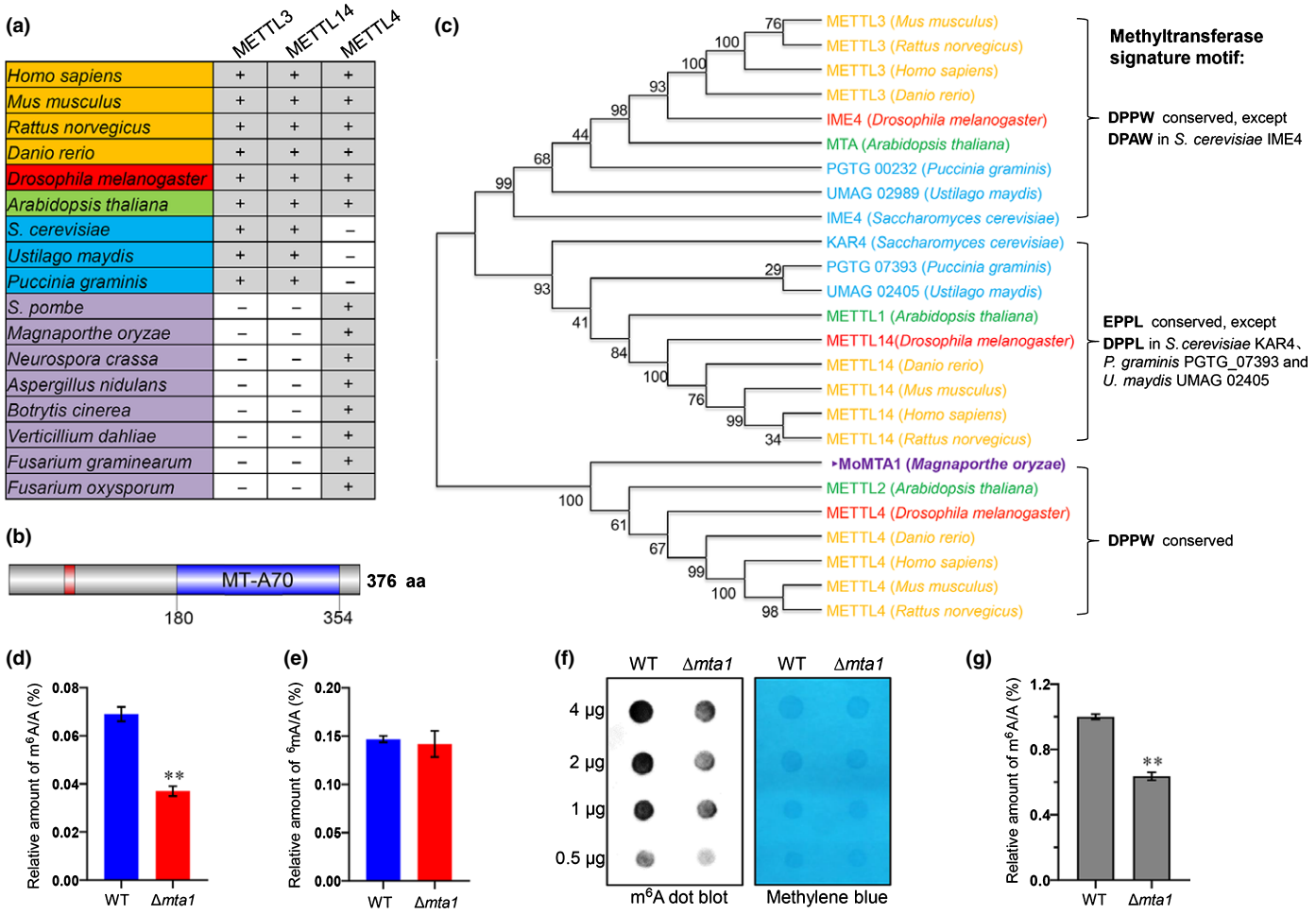

Fig. 1 MTA1 is involved in m^{6}A RNA methylation in *Magnaporthe oryzae*. (a) Distribution of human METTL3, METTL14 and METTL4 homologue proteins in different organisms. (b) *Magnaporthe oryzae* MTA1 protein conserved domains predicted using a simple modular architecture research tool (SMART). The MTA1 protein contains an *S*-adenosylmethionine-binding domain MT-A70. (c) Phylogenetic analysis of *M. oryzae* MTA1 with the homologues and different RNA methyltransferases from other species using molecular evolutionary genetics analysis v.5 (MEGA5). Bootstrap analyses were performed with 1000 iterations, and support for each node is displayed. Numbers at the nodes indicate the bootstrap values on neighbour joining analysis. (d) Methylation level of m^{6}A RNA in the wild-type (WT) and Δ*mta1* was detected using an RNA methylation quantitative kit. Error bars represent standard errors, and asterisks represent significant differences (**, $P < 0.01$). (e) Methylation level of ^{6}mA DNA in the WT and Δ*mta1* was detected using a DNA methylation quantitative kit. Error bars represent standard errors. (f) RNA dot blot analysis of m^{6}A levels in the WT and Δ*mta1* using a specific m^{6}A antibody. Total RNA from the WT and the Δ*mta1* mutant were extracted and spotted onto Hybond™-N+ membranes and incubated with an m^{6}A antibody, then detected using the enhanced chemiluminescence (ECL) detection system. Methylene blue staining served as a loading control. (g) Quantification of RNA blot analysis using ImageJ software. The level of RNA blot signal (4 μg loading) in (f) was used for analysis. Error bars represent standard errors, and asterisks represent significant differences (**, $P < 0.01$).

We used the split-PCR strategy for the deletion of *MTA1*. The deletion mutants were screened using PCR and confirmed by Southern blotting (Fig. S1a,b). Two knockout mutants, mta1-1 and mta1-2, were used for further analysis. To determine whether MTA1 is required for m^{6}A RNA methylation or ^{6}mA DNA methylation in *M. oryzae*, we compared total m^{6}A RNA methylation levels between the wild-type strain and the Δ*mta1* mutant. The amount of m^{6}A RNA in the Δ*mta1* mutant was 0.037 ± 0.002% of the total RNA, which was 53.6% of that in the wild-type (0.069 ± 0.003% of the total RNA), indicating a significant reduction of m^{6}A RNA modification (Fig. 1d). The amount of ^{6}mA DNA in the Δ*mta1* mutant was comparable with that in the wild-type (Fig. 1e), suggesting that MTA1 maybe not be involved in ^{6}mA DNA methylation. We also detected the levels of m^{6}A modification using m^{6}A mRNA dot blots, which confirmed that the m^{6}A RNA methylation level was significantly reduced in the Δ*mta1* mutant compared with the wild-type (Fig. 1f,g). Therefore, we considered *M. oryzae* MTA1 to be involved in m^{6}A methylation.

Deletion of *MTA1* affects vegetative growth and conidial formation

Expression patterns of *MTA1* during different developmental stages of *M. oryzae* showed that *MTA1* expression was not changed significantly (two-fold) in all tested developmental tissues (mycelium, conidium, appressorium, and infection hypha) by qRT-PCR, indicating that it plays a universal role in different stages of development and infection (Fig. S2).

Then we compared the colony size of the mutants with size of the wild-type on the oatmeal tomato agar (OTA) plates. We observed that the colony diameter of Δ*mta1* was significantly reduced (Fig. S3a,b), reflected by the reduction in the cell lengths in apical hyphal cells stained by calcofluor white (CFW) (Fig. S3c,d). We also observed the conidia formation on the conidiophore of the Δ*mta1* mutant and found that it formed more sparse conidia compared with that formed by the wild-type (Fig. S3e). As a consequence, the Δ*mta1* mutant only produced *c.* 47.3% of the conidia produced by the wild-type (Figs S3f). The Δ*mta1* mutant was also abnormal in conidial cell number (Fig. S3g,h). These results showed that deletion of *MTA1* affects the asexual development of *M. oryzae*.

MTA1 is important for pathogenicity

To investigate whether *MTA1* is involved in infection of *M. oryzae*, we performed the virulence test on rice seedlings and barley leaves. The result showed a significant virulence reduction of the Δ*mta1* mutant on both host plants (Fig. 2a,b). We also tested if the invasive growth of the mutant was affected by inoculating the mycelial plugs onto the wounded rice seedlings, and observed that the Δ*mta1* mutant caused smaller lesions compared with that of the wild-type (Fig. 2c). To determine why the Δ*mta1* reduced in virulence, we observed the cellular infection process. We found that the Δ*mta1* mutant was severely defective in penetration and invasive growth in barley epidermal cells (Fig. 2d,e). Collectively, these results showed that MTA1 is important for pathogenicity by affecting appressorial penetration and invasive growth.

MTA1 is required for appressorium turgor pressure

Defects in appressorial penetration are usually caused by the failure to accumulate enough turgor pressure, and the appressorium formation was normal in the Δ*mta1* mutant (Fig. 3a,b), so we speculated that the mutant appressoria were not fully functional. Therefore, we detected the turgor pressure of the Δ*mta1* mutant appressoria through a cytorrhysis assay. As shown in Fig. 3(c), when treated with external PEG8000, the appressoria of Δ*mta1* collapsed much more easily, suggesting a serious reduction of turgor accumulation.

In *M. oryzae*, appressorial turgor accumulation suggests an appressorial maturation, which is demonstrated by the effective utilisation of conidial glycogen and lipid. We subsequently examined whether the utilisation of conidial glycogen and lipid in the Δ*mta1* mutant was affected. When the lipid droplets were stained using Nile Red, we could observe that their utilisation during appressorium formation and maturation was retarded in the Δ*mta1* mutant, demonstrated by a large number of lipid droplets that remained in the appressorium at 24 hpi (Fig. 3d,f). Similarly, when glycogen was stained using I_2/KI solution, we also observed severe defects in the degradation of glycogen during appressorial maturation (Fig. 3e,g). These results indicated that MTA1 is required for glycogen and lipid degradation, which is important for utilisation of conidial storage to form a functional appressorium in *M. oryzae*.

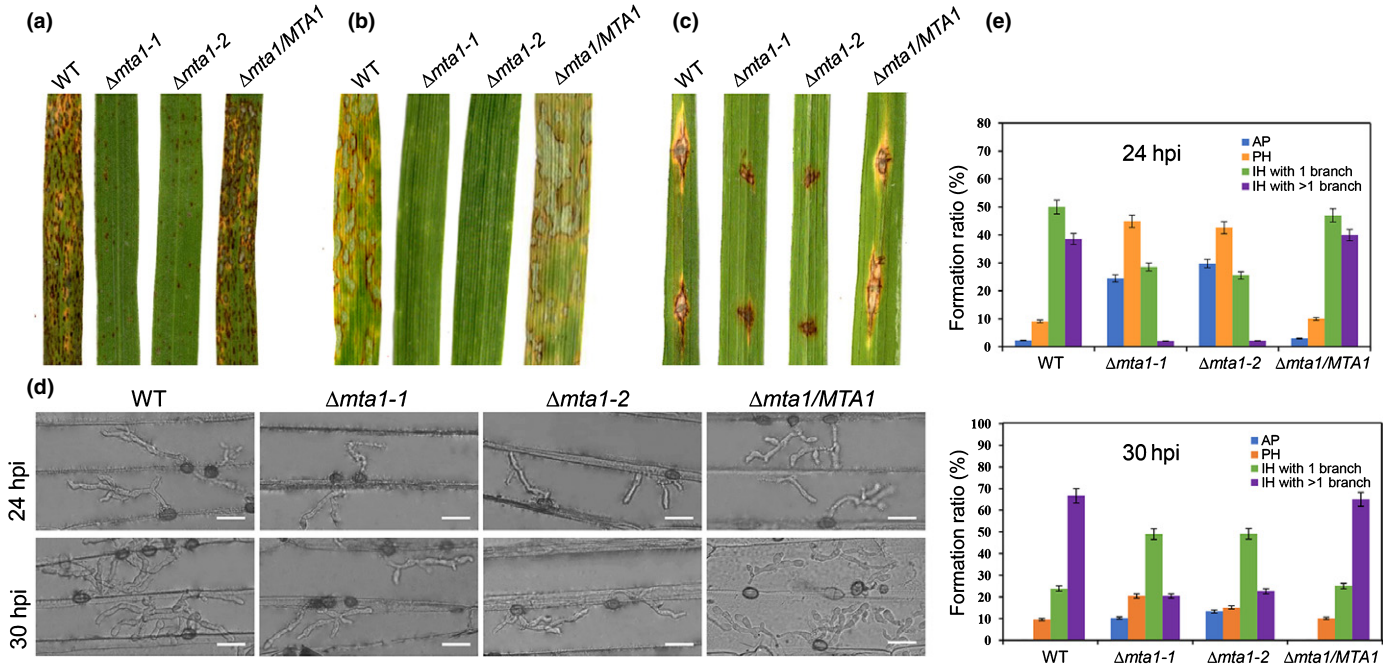

Fig. 2 MTA1 is important for pathogenicity of *Magnaporthe oryzae*. (a) Spray assay for disease development on rice seedlings. Lesions formed on rice leaves were infected by the indicated strains at 5 d post-inoculation (dpi). (b) Spray assay for disease development on barley leaves. Lesions formed on barley leaves at 5 dpi. (c) Lesions formed on wounded rice leaves. Hyphal agar plugs (5 mm in diameter) were placed onto rice leaves with treatment of wounds and incubated for 4 d. (d) Penetration and infection hyphae of wild-type (WT) and Δ*mta1* mutant were examined at 24 and 30 h post-inoculation (hpi). Bar, 20 μm. (e) Statistical data of the different structures at 24 and 30 hpi. AP, appressoria; Δ*mta1-1* and Δ*mta1-2*, deletion mutans of MTA1; Δ*mta1/MTA1*, complementation strain of *MTA1*; IH, invasive hyphae; PH, primary hyphae. Error bars represent standard error (SE), $P < 0.05$ (1SE).

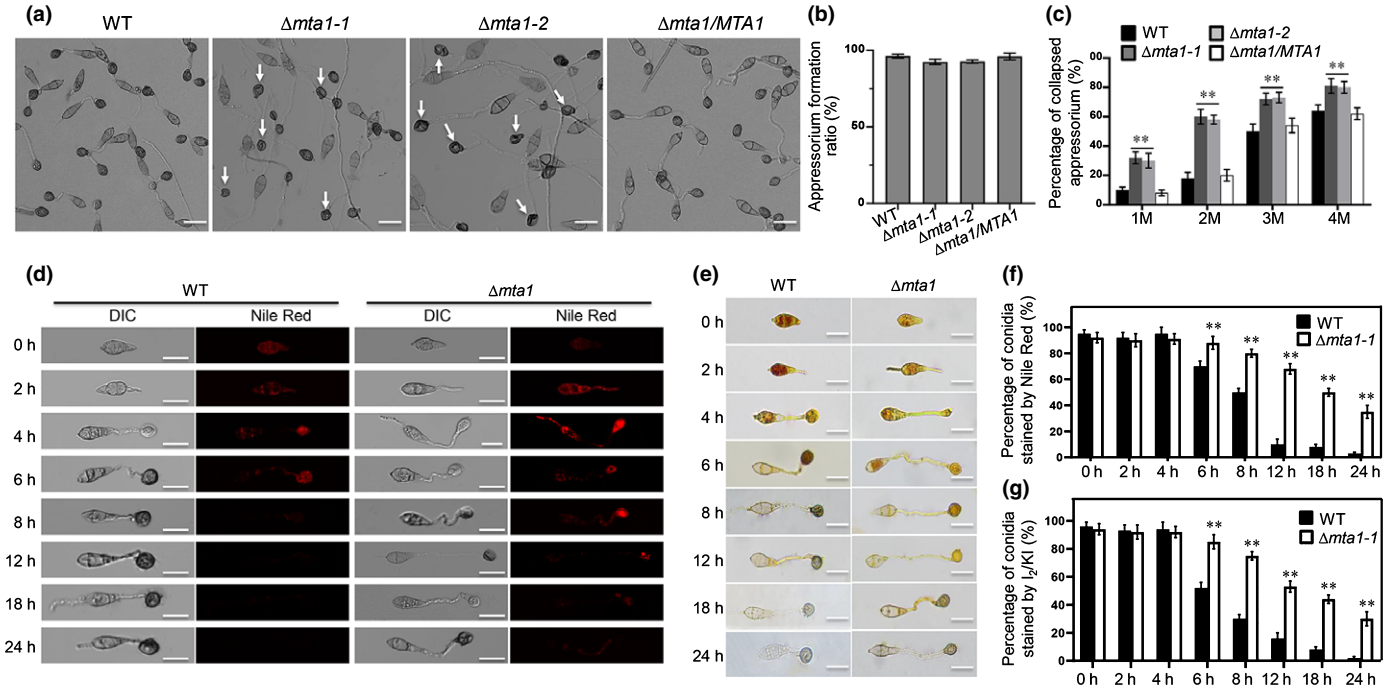

Fig. 3 *MTA1* disruption affects the functions of appressoria. (a) Appressorium formation assay. Spore suspensions were incubated on hydrophobic surfaces and observed at different time points. White arrows indicate appressoria. Bar, 20 μm. (b) Appressorium formation rates at different time points ($n > 100$). Error bars represent standard errors. (c) Cytorrhysis assay for appressorium turgor pressure. Drops of conidial suspension were placed on the hydrophobic surface of a coverslip and treated with the indicated concentration of polyethylene glycol 8000 (PEG8000) at 24 h post-inoculation (hpi). Error bars represent standard errors, and asterisks represent significant differences (**, $P < 0.01$). For (a–c): WT, the wild-type strain; Δ*mta1-1* and Δ*mta1-1*, deletion mutants of MTA1; Δ*mta1/MTA1*, complementation strain of *MTA1*. (d) Observation of lipid utilisation during appressoria formation. Conidia and appressoria were stained with Nile Red and photographed at different time points. Bar, 20 μm. (e) Observation of glycogen utilisation during appressoria formation. The spores or appressoria were stained with I_2/KI and photographed at different time points. Bar, 20 μm. (f) Statistics showing the percentage of conidia or appressoria containing glycogens during lipid metabolism development in the wild-type (WT) and Δ*mta1*. Error bars represent standard errors, and significant differences compared with the WT are indicated by an asterisk ($n > 100$; **, $P < 0.01$). (g) Statistics showing the percentage of conidia or appressoria containing lipid bodies during glycogens metabolism development in WT and Δ*mta1*. Error bars represent standard errors, and significant differences compared with the WT are indicated by an asterisk ($n > 100$; **, $P < 0.01$).

Deletion of *MTA1* resulted in increased sensitivity to various stresses

Next, we evaluated the effect of *MTA1* disruption on stress tolerance in *M. oryzae*. The results showed that the Δ*mta1* mutant was more sensitive to a series of stresses or conditions, including the cell wall perturbing reagents of CFW (0.1 mg ml^{-1}), Congo Red (CR, 0.2 mg ml^{-1}) and sodium dodecyl sulfate (SDS, 0.005%), the osmotic stresses of NaCl (0.5 M) and sorbitol (1 M), at different pH values of 5.8, 6.8, 7.8, as well as oxidative stress of H_2O_2 (10 mM) (Fig. S4a,b). These findings suggest that *MTA1* plays an important role in stress response.

Magnaporthe oryzae Δmta1 mutant activates host immune responses

To determine why the Δ*mta1* mutant is defective in invasive growth, we tested whether the mutant could activate host immune responses. Plant immunity responses induced by pathogens are usually associated with the accumulation of reactive oxygen species (ROS). When stained with 3,3′-diaminobenzidine (DAB), we observed massive ROS accumulated in the Δ*mta1* mutant-infected host cells, compared with less detected in the wild-type strain-infected ones (Fig. S5a,b). When we used diphenylene iodonium (DPI, 0.4 μM), an antioxidant as NADPH oxidase inhibitor, to treat the plant epidermis cells, the defect of Δ*mta1* invasive growth was partially recovered (Fig. S5c). These data suggest that MTA1-mediated m6A is involved in responding to host oxidative stress.

The qRT-PCR analysis showed that the transcriptional levels of *M. oryzae* two detoxification genes, *KAR2* and *LHS1*, were significantly reduced in Δ*mta1* (Fig. S5d). We also examined the expression levels of several rice immune responsive genes, most of which were significantly induced by the Δ*mta1* mutant strain, especially *OsLYP4*, *OsPBZ1* and *OsPR1* (Fig. S5e). These results showed that MTA1 plays role in suppressing host innate immunity during fungal infection.

MeRIP-seq detects m^6A modification during appressorium formation of *M. oryzae*

To understand the biological impact of m^6A in *M. oryzae* and the underlying mechanism, particularly associated with appressorium formation, we performed m^6A sequencing using appressoria formed by an *M. oryzae* conidial suspension of wild-type and the Δ*mta1* mutant at 12 hpi. We used MeRIP-seq technology to

detect m^{6}A. After QC and principal component analysis (PCA) (Fig. S6a–e), we compared the m^{6}A peaks detected between IP samples and input samples as background. From these data, we detected m^{6}A peaks and identified 14 762 and 14 142 sites of methylated poly(A) mRNAs derived from 7880 and 7817 genes, respectively, in wild-type samples in wild-type and Δ*mta1* samples (Fig. S6g; Table S3).

To understand the overview of m^{6}A peaks crossing the genome in *M. oryzae*, we first performed analysis using the m^{6}A peaks detected in wild-type samples. Intriguingly, m^{6}A methylation preferably occurs in the genes with 50–60% CG content (Fig. 4a), and within the genes with a longer length of transcripts, compared with that in the whole genome of *M. oryzae* (Fig. 4b). Further data analysis identified several motifs sequences as conserved consensus sequences among all the m^{6}A peaks in wild-type strain, for instance, UGCUGACAUU is the most frequent putative motif (Fig. 4c).

To study the effect of the complex function of the gene, the significance of the enrichment peak of m^{6}A detected in the wild-type and Δ*mta1* mutant was tested using the *t*-test. The results

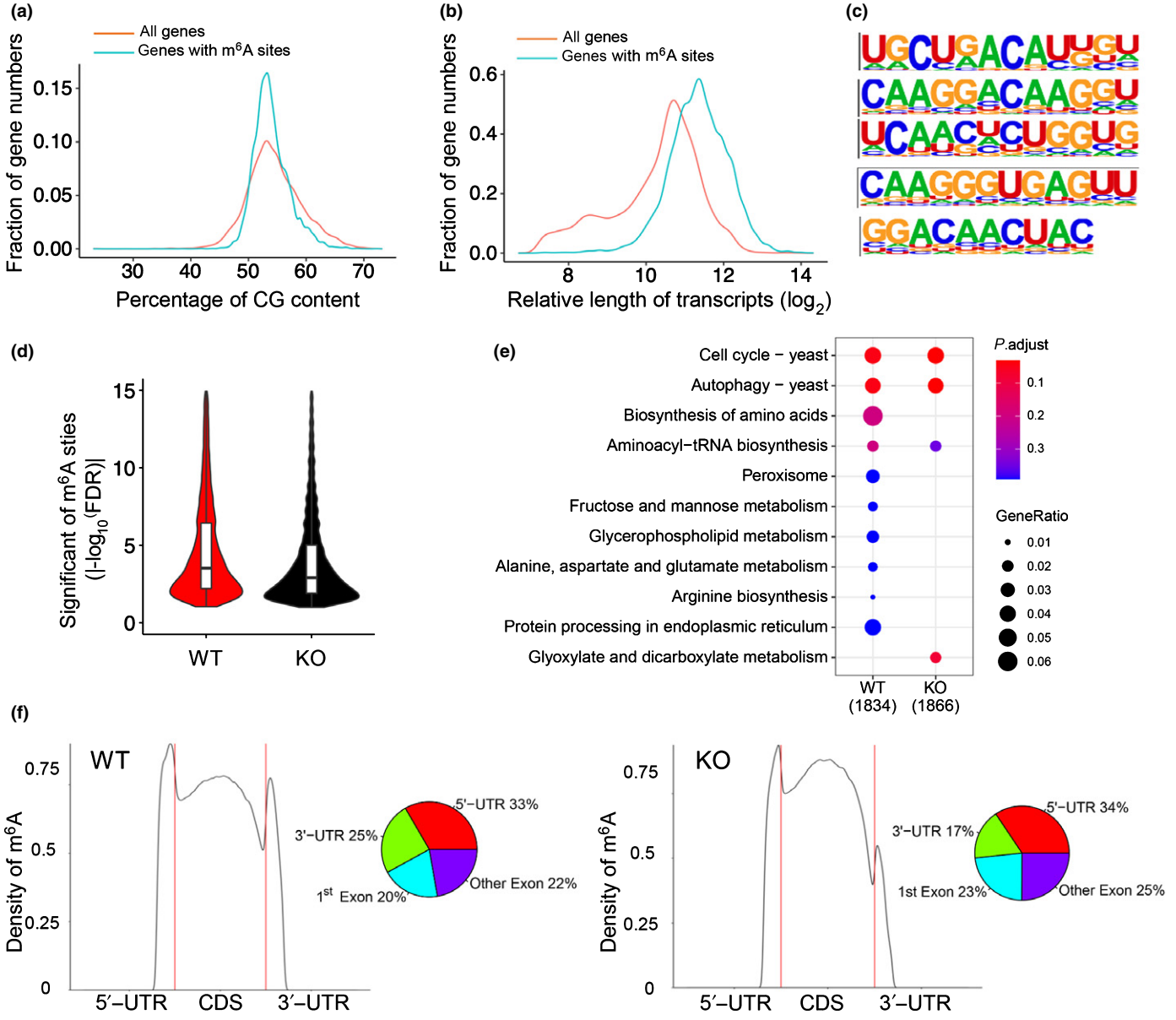

Fig. 4 Genome-wide identification of all and MTA1-mediated m^{6}A modification in *Magnaporthe oryzae*. (a) Line plots showing the percentage of CG content of all genes carrying m^{6}A modifications detected using m^{6}A-seq. (b) Line plots showing the relative length of transcripts in all genes carrying m^{6}A modifications. (c) Consensus sequences identified within m^{6}A peaks of the poly(A) RNAs of *M. oryzae* from the wild-type strain and the Δ*mta1* mutant. (d) Distribution of enrichment scores detected in the poly(A) RNAs of wild-type strain and the Δ*mta1* mutant. In each plot, the horizontal line inside the box shows the median, quartiles with whiskers indicate minimum and maximum values, and the width of the shaded areas indicates the distribution of the data. (e) Most impacted Kyoto Encyclopedia of Genes and Genomes (KEGG) metabolism pathways of the methylated RNAs detected in wild-type and the Δ*mta1* mutant. (f) Distribution of m^{6}A along the whole mRNA transcripts of *M. oryzae* detected in the wild-type strain and the Δ*mta1* mutant.

showed that there was a significant difference between them, indicating that the complex function of the gene was seriously affected by the MTA1-mediated m^{6}A modification (Fig. 4d). Enrichment analysis of genes with detected m^{6}A peaks indicated that many metabolic pathways are tightly associated with m^{6}A methylation, which involves cell cycle, autophagy, peroxisome, glycerophospholipid metabolism and arginine biosynthesis (*P*-adj < 0.1). Pathways of peroxisome, glycerophospholipid metabolism and arginine biosynthesis are much less enriched by m^{6}A modified genes in the Δ*mta1* mutant, suggesting that much of the effect on metabolic pathways and gene functions is mediated by MTA1 (Fig. 4e). Further analysis compared enrichment of the peaks in the wild-type and Δ*mta1* mutant, we defined that the genes were significantly reduced in m^{6}A modification. Compared with the wild-type, we identified 659 hypomethylated m^{6}A peaks covering 595 genes in the Δ*mta1* mutant (Table S4) that could be affected by MTA1 catalytic activity. After segment normalisation by the total length of each gene portion, we found that m^{6}A modification in the wild-type was significantly enriched within the 5′ UTR and 3′ UTR regions. While, in the Δ*mta1* mutant, m^{6}A peaks at the 3′ UTR were significantly reduced (Fig. 4f), suggesting that MTA1 was more important for m^{6}A modification of 3′ UTR.

MTA1 deletion alters expression pattern of genes during appressorium formation

To understand the impact of m^{6}A to gene expression at the transcriptional level, we performed comparative transcriptome analysis using the same material harvested from the 12 hpi appressorium samples. By performing PCA and clustering, we observed a distinct pattern of the global transcriptome of *M. oryzae* between the wild-type and Δ*mta1* mutant samples (Fig. 5a), suggesting that m^{6}A modification caused many effects on gene expression. By performing differentially expressed gene (DEG) analysis, we identified 706 and 262 genes as significantly upregulated (> 1.5-fold) and downregulated genes (< −1.5-fold), respectively (Fig. 5b,c; Table S5).

For integrative analysis to investigate impact of reduced m^{6}A modification on gene expression, we found that, among the 595 hypomethylated mRNAs in the Δ*mta1* mutant, 114 corresponding genes were transcriptionally upregulated, and 35 genes were transcriptionally downregulated (Fig. 5d), suggesting that the Δ*mta1* mutant predominantly conferred an increase in mRNA.

Gene ontology (GO) enrichment analysis suggested that the biological processes associated with membrane function and transmembrane transport were significantly enriched by de-repressed genes in the Δ*mta1* mutant, suggesting that m^{6}A directly modulates genes involved in these processes by degradation of the mRNA of target genes (Fig. 5e). Interestingly, KEGG pathway enrichment analysis showed that genes that were transcriptionally de-repressed in the Δ*mta1* mutant were significantly and specifically enriched in metabolic pathways related to starch and sucrose metabolism, biosynthesis of secondary metabolites, valine, leucine and isoleucine biosynthesis and autophagy, which are tightly associated with appressorium development in *M. oryzae* (Fig. 5f). By contrast, genes transcriptionally activated by MTA1 were specifically enriched in metabolic pathways associated with ABC transporters, ether lipid metabolism and glycerophospholipid metabolism (Fig. 5f). Localisation prediction analysis suggested that transcripts specifically mediated by MTA1 in *M. oryzae* were mainly encoded by the genes whose final protein products may localise in the cytoplasm, cell membrane, nucleus, as well as extracellularly, which was consistent with the GO analysis (Fig. 5g). Taken together, these results suggested that gene expression at the transcriptional level is significantly affected by m^{6}A-mediated modification, particularly as a repression mechanism to modulate genes involved in metabolic pathways, especially autophagy.

MTA1 regulates expression of *ATG* genes during appressorium formation

There are in total 32 autophagy-related genes annotated in the genome of *M. oryzae*, and many of them are tightly associated with appressorium development and pathogenicity (Kershaw & Talbot, 2009). We specifically focused on *ATG* family genes and found 32 m^{6}A sites located in transcripts of 23 *ATG* genes. Strikingly, m6A modification on 10 ATG mRNAs (ATG1, ATG4, ATG5, ATG8, ATG11, ATG12, ATG13, ATG15, ATG17 and ATG18) was mediated by MTA1 (FDR < 0.05), as their mRNA m^{6}A peaks were reduced in the Δ*mta1* mutant (Fig. 6a,b; Table S6). Further gene expression profiling suggested that some *ATG* genes, such as *ATG1*, *ATG4*, *ATG5*, *ATG8*, *ATG11*, *ATG15*, *ATG16*, *ATG17*, *ATG26* and *ATG27*, were de-repressed in the Δ*mta1* mutant, suggesting that MTA1-mediated m^{6}A modification mainly modulated the expression of *ATG* family genes by mRNA degradation (Fig. 6c). These results suggested that MTA1-mediated m^{6}A modification affected autophagy, which is vital for appressorium formation and virulence of *M. oryzae*.

MTA1 mediates the stability of Atg8 mRNA in a m^{6}A dependent manner

The m^{6}A-Seq and RNA-seq integrative analysis indicated that the Atg8 transcript might be an important target of MTA1 for regulation of autophagy. To test this possibility, we first used an online tool SRAMP (http://www.cuilab.cn/sramp) to predict the possible exact methylation sites of m^{6}A RNA in transcripts of *MoATG8*. Interestingly, a putative m^{6}A site A982 is located in 3′ UTR region with very high confidence, which is consistent with our m^{6}A-seq result (Figs 6b, 7a). We subsequently mutated this site by changing A to C and transformed the mutated gene into the Δ*moatg8* mutant. Subsequent transformant Δ*atg8*/*ATG8*^{A982C}(Δ*atg8*/*GFP:ATG8*^{A982C}) was used for further analysis. MeRIP-qPCR analysis showed that, compared with wild-type, the level of m^{6}A modification on the *ATG8* mRNA transcript in overexpression strain OE-MTA1 was evidently increased, but significantly decreased in Δ*mta1* and Δ*atg8*/*ATG8*^{A982C} mutants (Fig. 7b). These results indicated that MTA1 may regulate m^{6}A modification of MoATG8 at the A982 site.

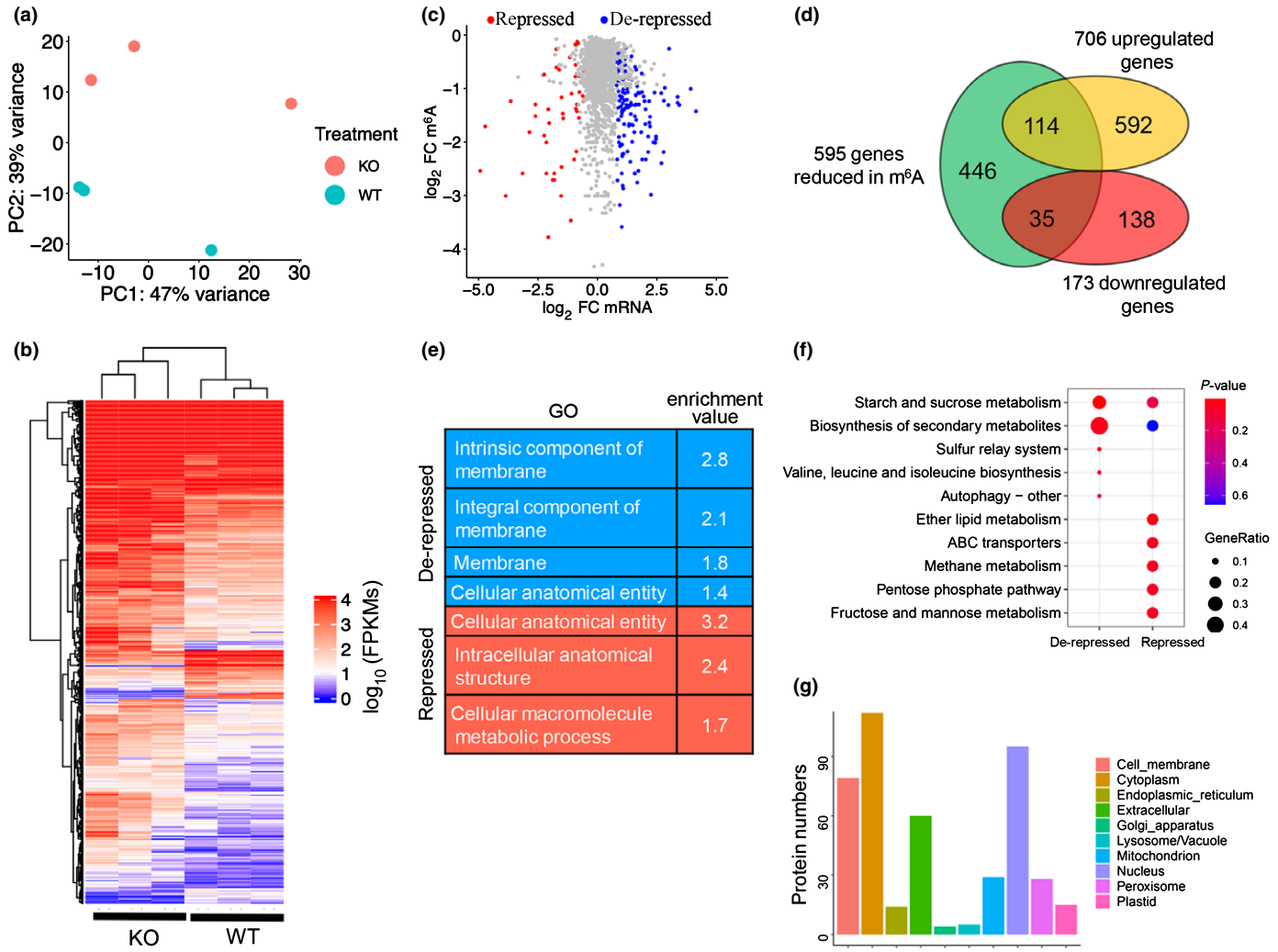

Fig. 5 Integrative analysis of m^{6}A-seq and RNA-seq identified transcripts affected by MTA1. (a) Plot showing principal component analysis (PCA) to demonstrate discriminated global transcriptional patterns between the wild-type (WT) and the Δ*mta1* mutant stain (KO). (b) Heatmap showing relative levels of transcripts of all genes of WT strain and the KO in RNA-seq. (c) Plot showing integrative analysis of m^{6}A-seq and RNA-seq to analysis de-repressed ($log_2|FC| > 0.83$) and repressed ($log_2|FC| < 0.83$) transcripts containing significantly altered m^{6}A modification. (d) Venn diagram showing numbers of transcriptionally de-repressed or repressed genes significantly less m^{6}A modified. (e) Table showing Gene Ontology (GO) terms as biological processes and molecular functions enriched by transcriptionally de-repressed or repressed affected by altered m^{6}A modification mediated by MTA1. The enrichment values represent as $-log_{10}$(*P*-value), cut-off: *P*-value < 0.05. (f) KEGG metabolism pathways enriched in genes transcriptionally de-repressed or repressed with reduced m^{6}A in the Δ*mta1* mutant. (g) Bar plot showing numbers of predicted localisation of proteins encoded by the differentially changed transcripts with reduced m^{6}A in the Δ*mta1* mutant.

Next, we explored whether MTA1 could affect the stability of Atg8 through RNA methylation. qRT-PCR results showed that, compared with the wild-type, the relative transcript abundance of *ATG8* mRNA in overexpression strain *OE-MTA1* decreased significantly, but was upregulated in Δ*mta1* and Δ*atg8*/*ATG8*$^{A98 2C}$ mutants (Fig. 7c). We also designed a strand-specific qRT-PCR to reveal the transcripts of *ATG8* containing introns, which could demonstrate the transcription rate (pre-mRNA) of ATG8. The results showed that the transcription rate of ATG8 in WT, Δ*mta1* and Δ*atg8*/*ATG8*$^{A98 2C}$ was not significantly different (Fig. 7d), suggesting that m^{6}A did not affect the expression of Atg8 mRNA. At the same time, western blot results showed that the *MTA1* deletion or the m^{6}A modification site mutation not only affected the mRNA stability of *ATG8*, but also affected its protein level (Fig. 7e,f). In conclusion, we confirmed that *ATG8* mRNA is the target of MTA1, and that MTA1 can mediate the stability of Atg8 mRNA in an m^{6}A-dependent manner.

MTA1 mediates autophagy in an m^{6}A-dependent manner

Previous studies have shown that Atg8 is a necessary factor for autophagic cell death in *M. oryzae* and that deletion of *ATG8* will directly lead to the autophagy defect (Veneault-Fourrey *et al.*, 2006). As MTA1 can mediate the mRNA stability of *ATG8* in a mRNA m^{6}A-dependent manner, we investigated whether MTA1 could regulate autophagy. We transformed GFP-Atg8 into WT and Δ*mta1* strains respectively and then treated the mycelia of the transformants with nitrogen starvation. The content and

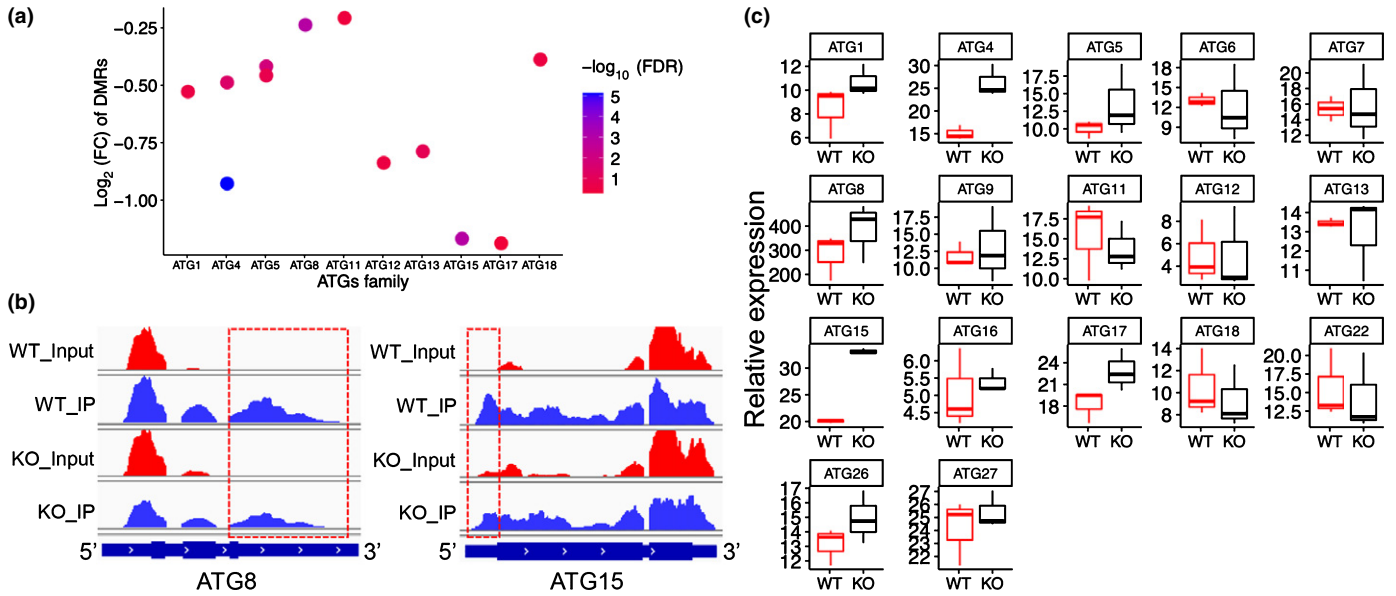

Fig. 6 Relative transcript abundance of m^{6}A modified transcripts derived from autophagy-related genes are severely affected by MTA1. (a) Plot showing fold change values of significantly abolished m^{6}A modification in transcripts of autophagy-related genes affected by MTA1. Colours indicating degree of significance of difference between wild-type (WT) and the Δ*mta1* mutant (KO). (b) Integrative genomics viewer (IGV) plots showing examples of m^{6}A peaks at transcript of autophagy-related genes in *Magnaporthe oryzae*. Red reads originate from m^{6}A IP libraries of WT and blue reads originate from m^{6}A IP libraries of the KO. Y-axis represents normalised numbers of reads count. Red boxes indicate that m^{6}A peaks of the transcripts in Δ*mta1* are lower than in the WT. (c) Boxplots showing the relative expression as fragments per kilobase of exon per million mapped fragments (FPKMs) of transcripts encoded by the autophagy-related genes in *M. oryzae* in RNA-seq, and comparing WT strain and the KO. The horizontal lines (mean values of replicates), boxes (upper |0.75| and lower |0.25| quantiles), whiskers (minimum/maximum value). DMRs, differentially methylated regions; FC, fold change; FDR, false discovery rate; FPKM, Fragments per kilobase of exon model per million mapped fragments; IGV, integrative genomics viewer.

localisation of GFP-Atg8 labelled autophagosomes were observed using a fluorescence microscope. The results showed that 90% of autophagosomes in the wild-type were located in vacuoles after 5 h of nitrogen starvation, while in the Δ*mta1* mutant nearly 30% of the autophagosome remained in the cytoplasm, but not in the vacuole (Fig. 8a,b). These results suggested that the regulation of autophagy is severely disordered in the Δ*mta1* mutant.

In addition, we measured the autophagy level by western blot. The degree of autophagy was evaluated by calculating the ratio of free GFP amount to GFP-Atg8 plus free GFP amount. The results suggested that, compared with the wild-type, the Δ*mta1* mutant displayed higher autophagy induction and degradation. Surprisingly, we found that the level of autophagy in the mutant Δ*atg8*/*ATG8*^{A982C} was almost the same as that in the Δ*mta1* mutant (Fig. 8c,d). In conclusion, MTA1 can be involved in maintaining the autophagy homeostasis of *M. oryzae* in an m^{6}A-dependent manner.

MTA1 mediates autophagosome formation during appressorium formation stage

The above results showed that the *MTA1* deletion could lead to defects in the utilisation of conidial storage during appressorium maturation, which may be related to the role of MTA1 in autophagy. To detect the appressorial autophagy process, the autophagy level of appressoria formation was observed by fluorescence microscope. At the initial stage, GFP-Atg8-labelled autophagosomes mainly accumulated in the spores of the wild-type. During appressorium formation and maturation, the autophagosomes of GFP-Atg8-labelled in the WT strain was normal, but was significantly increased in the Δ*mta1* mutant (Fig. 8e,f). The autophagosome number in the mutant Δ*atg8*/*GFP:ATG8*^{A982C} was almost the same as that in the Δ*mta1* mutant (Fig. 8e,f). Therefore, we believe that, during autophagy processes induced by nitrogen starvation or during appressorium formation, the deletion of *MTA1* will lead to a decrease in m^{6}A modification and decreased mRNA degradation of Atg8, resulting in its protein accumulation in the cells, therefore affecting the autophagosome number and autophagy homeostasis. This is consistent with above conclusion that MTA1 can participate in maintaining the autophagy homeostasis of *M. oryzae* in dependence of m^{6}A.

The m^{6}A site A982 of ATG8 mRNA is important for conidiation and virulence

To study the effect of the m^{6}A methylation site at 982 of ATG8 on the growth and sporulation of *M. oryzae*, we measured the growth rate and sporulation ability of wild-type P131, Δ*atg8*, Δ*atg8*/*ATG8*^{A982C} and Δ*atg8*/*ATG8* strains. The results showed that there was no significant difference in growth rate among these strains, but there were differences in sporulation ability (Fig. 9a,c). The sporulation ability of the Δ*atg8*/*ATG8*^{A982C} mutant was significantly lower than that of wild-type and complement strains, even though it was much higher that of Δ*atg8* (Fig. 9c). These results indicated that the A982 m^{6}A site of

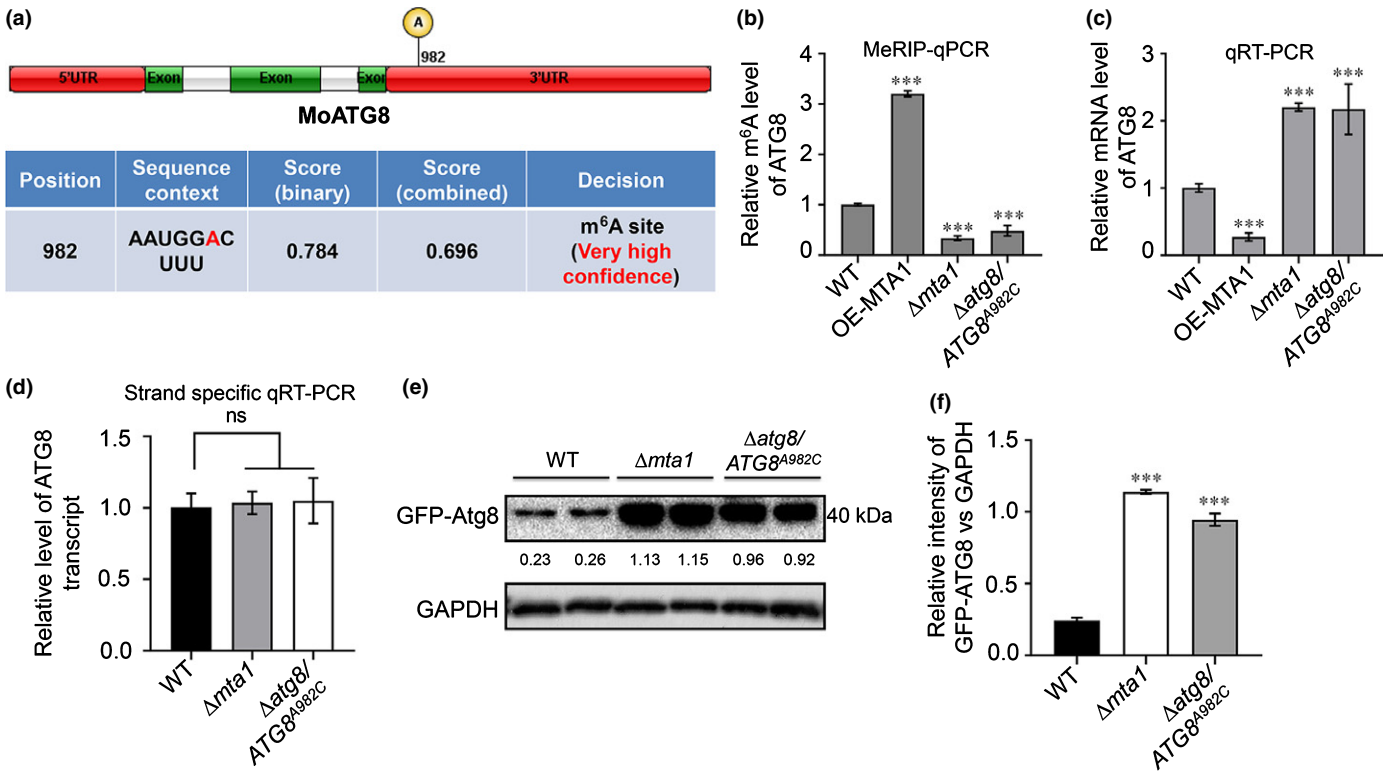

Fig. 7 MTA1 regulates the autophagy in an m^{6}A-dependent manner. (a) Online prediction of the m^{6}A RNA methylation site of MTA1 the sequence-based RNA adenosine methylation site predictor SNAMP. (b) Methylated RNA immunoprecipitation-qPCR (MeRIP-qPCR) analysis of m^{6}A levels of autophagy-related protein (ATG)8 in *M. oryzae*. The appressorium samples of the wild-type (WT) and Δ*mta1* mutant were used for m^{6}A-IP assays by using an anti-m6A antibody. Subsequent MeRIP-qPCR was performed using IP assay products as the template. Error bars represent standard error (SE). ***, $P < 0.001$. (c) The mRNA level of *ATG8* was analysed by qRT-PCR. Means ± SE were calculated from three independent replicates. ***, $P < 0.001$. (d) Strand-specific qRT-PCR analysis. Total mRNA was used to perform reverse transcription using specific primer priming the intron region of *ATG8* (intron of actin gene *ACT1* was used as a control). qRT-PCR was then performed to amplify the *ATG8* intron to demonstrate the transcription rate of *ATG8*. Error bars represent SE. ns, no significance. (e) Expression of Atg8 protein was analysed by western blotting with anti-green fluorescent protein (GFP). Anti-glyceraldehyde-3-phosphate dehydrogenase (GAPDH) antibody was used for the control. (f) Relative intensity of GFP:ATG8 in WT and the Δ*mta1* mutant by comparison with the internal control GAPDH. Error bars represent SE. ***, $P < 0.001$; $P < 0.01$ (2SE)

ATG8 is related to conidia formation in *M. oryzae*. The appressorium formation ability of the Δ*atg8*/*ATG8*^{A982C} mutant was normal, but its appressorial turgor accumulation was significantly lower than that of wild-type and complement strains (Fig. 9d,e), suggesting a reduction in the penetration capacity.

To explore whether the A982 m^{6}A site of ATG8 mRNA is also related to the pathogenicity of *M. oryzae*, we tested the pathogenicity phenotypes of the wild-type P131, Δ*atg8*, Δ*atg8*/*ATG8*^{A982C} and Δ*atg8*/*ATG8* strains. As reported, the pathogenicity of strain Δ*atg8* was completely lost (Veneault-Fourrey *et al.*, 2006). Although the mutant strain Δ*atg8*/*ATG8*^{A982C} can cause disease, the number and area of necrotic lesions were significantly reduced, and the pathogenicity was seriously reduced (Fig. 9f). The results of rice scratch inoculation also showed that Δ*atg8*/*ATG8*^{A982C} significantly reduced the disease spot expansion and pathogenicity (Fig. 9g). Further analysis indicated that the infection process of mutant strain Δ*atg8*/*ATG8*^{A982C} slowed down significantly (Fig. 9h,i). In conclusion, the A982 m^{6}A site mutation of ATG8 resulted in a significant decrease in pathogenicity of *M. oryzae*, indicating that this m^{6}A site plays an important role in the process of infection.

Discussion

Many modifications have been found in eukaryotic RNA, however, the enzymes responsible for each modification and the biological role of these modified RNAs are still largely unknown. The m^{6}A writer has not been identified and analysed in filamentous fungi. In this study, we identified a putative m^{6}A writer MTA1 in *M. oryzae*. We found that MTA1 plays a key role in infection processes, especially appressorium-mediated penetration. Interestingly, autophagy-mediated appressorium maturation was severely blocked in the Δ*mta1* mutant. Transcripts of a series of *ATG* genes contained m^{6}A sites, which were relevant to their mRNA levels. As an example, we proved that the mRNA and protein accumulation of *MoATG8* is negatively regulated by m^{6}A, as a mechanism for the balance of appressorial autophagy. Taken together, our results revealed the functional importance of the m^{6}A methylation in autophagy regulation and infection of *M. oryzae*.

The most widespread candidates as m^{6}A methyltransferases belong to the MT-A70 family, such as human METTL3 and *S. cerevisiae* Ime4 (Clancy *et al.*, 2002; Fu *et al.*, 2014; Liu *et al.*, 2014). For a long period of time, the m^{6}A writer in filamentous

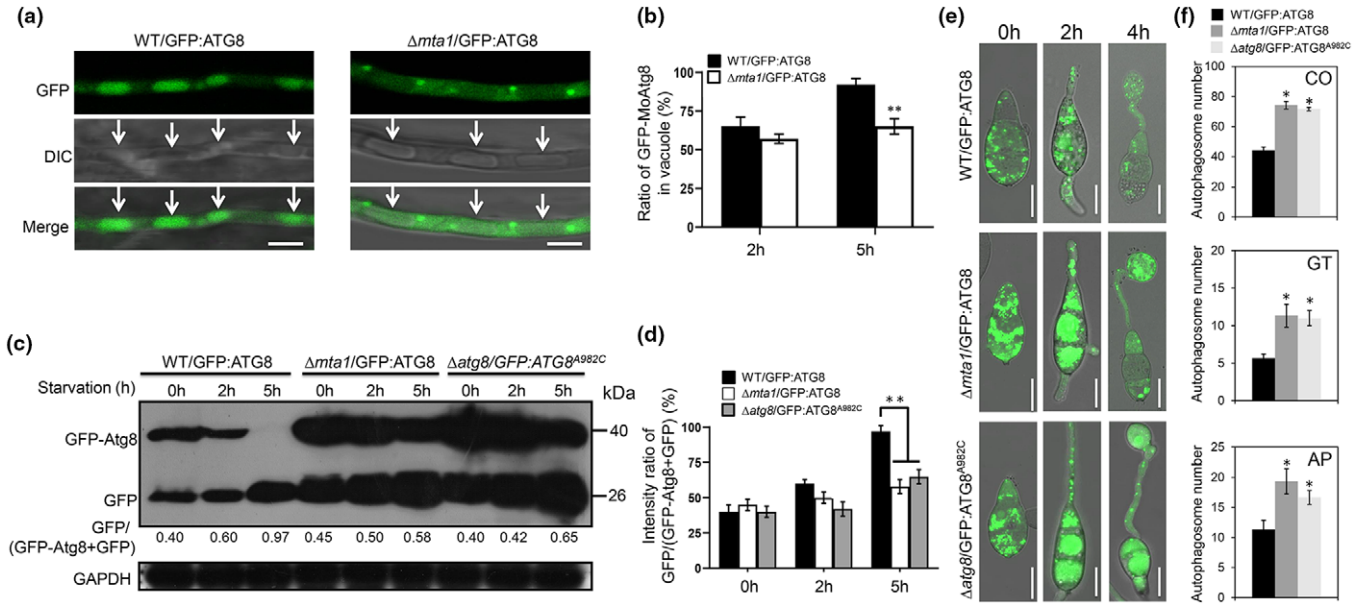

Fig. 8 MTA1 regulates the autophagy-related protein (ATG)8-mediated autophagy process. (a) Autophagic processes detected by observation of MoATG8 subcellular localisation. Wild-type (WT) and Δ*mta1* mutant strains transformed with green fluorescent protein (GFP)-Atg8 were cultured in MM-N medium for 5 h, and the autophagy intensity was observed using an Axio Observer A1 Zeiss inverted microscope. The arrows point to the vacuoles. Bars, 5 μm. (b) Autophagy intensity was assessed by means of translocation of GFP-Atg8 into vacuoles ($n = 100$). Error bars represent standard errors, and asterisks represent significant differences (**, $P < 0.01$). (c, d) Immunoblotting was performed with anti-GFP. Anti-glyceraldehyde-3-phosphate dehydrogenase (GAPDH) antibody was used for the control. The extent of autophagy was estimated by calculating the amount of free GFP compared with the total amount of intact GFP-Atg8 and free GFP (the numbers underneath the blot). Error bars represent standard errors, and asterisks represent significant differences (**, $P < 0.01$). (e) Cellular location of autophagosomes during infection-related appressoria development. Conidia of WT/*GFP:ATG8*, Δ*atg8*/*GFP:ATG8* and Δ*atg8*/*GFP:ATG8*^{A982C} were inoculated onto the hydrophobic interface and observed by epifluorescence microscopy at different times. Bar, 10 μm. (f) Bar chart showing mean autophagosome numbers present in conidia, germ tubes and appressoria at 0, 2 and 4 h after germination. Error bars represent standard errors, and asterisks represent significant differences ($P < 0.05$). AP, appressorium; CO, conidium; GT, germ tube.

fungi has not been found due to the lack of a METTL3/IME4 homologue. Recently, Shi *et al.* (2019) reported that PoIME4 (MGG 01492) is the homologue of *S. cerevisiae* IME4, however this conclusion is debatable. Based on phylogenetic analysis (Fig. 1a), the *M. oryzae* MGG 01492 (named MTA1 here) is much closer to human METTL4, another MT-A70 family protein, but not human METTL3, METTL14 or *S. cerevisiae* Ime4 (Clancy *et al.*, 2002; Liu *et al.*, 2014; Yadav & Rajasekharan, 2017). This inconsistency may due to the MTA70 domain sequence, but not the whole protein sequence, which was used as a query for homology comparison by the authors (Shi *et al.*, 2019). However, we also noticed that the results of Shi *et al.* (2019) indicated that Δ*Poime4* is indeed reduced in m6A level, which is consistent with our result (Fig. 1c–f). The METTL4 homologue proteins usually serve as DNA N^6-methyladenine (^{6}mA) writers in different organisms (Kweon *et al.*, 2019; Hao *et al.*, 2020). METTL4 has been also found to regulate RNA N^6,2′-*O*-dimethyladenosine (m^{6}Am) and m^{6}A methylation of U2 snRNA in *Drosophila* (Chen *et al.*, 2020; Goh *et al.*, 2020; Gu *et al.*, 2020), suggesting putative functions of this protein in RNA modification. METTL4 exhibits a weak enzymatic activity on DNA substrates, but strong enzymatic activity on RNA substrates in *Drosophila* (Gu *et al.*, 2020). Interestingly, our study found that the level of DNA ^{6}mA modification did not decrease in Δ*mta1*, suggesting that MTA1 maybe not important for ^{6}mA in *M. oryzae*. By contrast, Δ*mta1* significantly decreased in m^{6}A levels, and MeRIP-seq analysis detected 659 MTA1-dependent m^{6}A sites covering transcripts of 595 genes (Fig. 5d), indicating an important role of MTA1 in the m^{6}A of *M. oryzae*. MTA1 depletion resulted in a significant reduction of m^{6}A in 3′ UTR (Fig. 4f), suggesting an important role of MTA1 in 3′ UTR-related functions. Altogether, our study suggested that in *M. oryzae* and perhaps also in other filamentous fungi, m^{6}A is mediated by MTA1, the homologue of human METTL4 but not METTL3, which is quite different from other eukaryotic cells.

Our results suggested that loss of MTA1 resulted in a decrease in the m^{6}A levels of 10 *ATG* gene transcripts. The decrease in m^{6}A modification in the Δ*mta1* mutant resulted in de-repressing of gene expression, suggesting that MTA1-mediated m^{6}A modification regulates the mRNA stability of *ATG* genes through affecting mRNA degradation. Therefore, m^{6}A methylation was negatively correlated with the cellular mRNA levels of *ATG* genes. In mammals, m^{6}A affects multiple aspects of mRNA metabolism including splicing, degradation, nuclear export, folding and translation, whereas mRNA stability (degradation) is the best characterised role (Wang *et al.*, 2014). In plants, studies also showed that m^{6}A modification leads to instability of mRNA (Shen *et al.*, 2016; Duan *et al.*, 2017; Zhou *et al.*, 2019). For example, in Arabidopsis, FIP37-mediated m^{6}A methylation leads to mRNA instability (Shen *et al.*, 2016), while ALKBH10B-mediated m^{6}A de-methylation increases mRNA stability (Duan *et al.*, 2017). By contrast, several studies also showed an

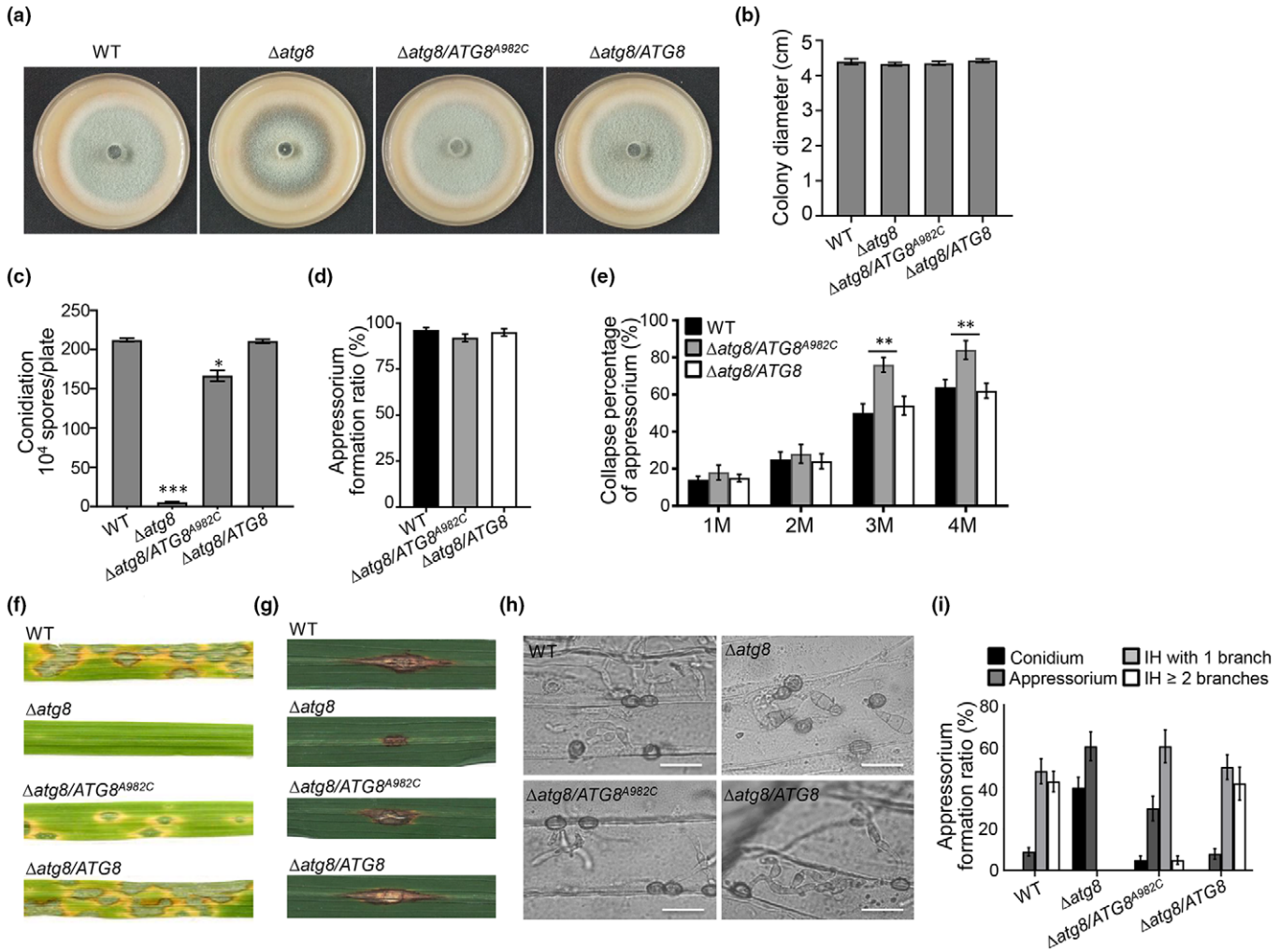

Fig. 9 The A982C m^{6}A site mutation in autophagy-related protein (ATG)8 transcripts affects *Magnaporthe oryzae* development and virulence. (a) Colony growth of the Δ*atg8/ATG8*^{A982C} strain. The indicated strains were cultured on oatmeal tomato agar (OTA) plates at 28°C for 5 d. (b) Colony diameter. Error bars represent standard errors. (c) Conidiation capacity. Conidia were collected from strains grown on OTA plates (Φ = 6 cm). Means and standard errors were calculated from three independent experiments ($n > 100$). Significant differences compared with the wild-type are indicated by an asterisk (*, $P < 0.05$; ***, $P < 0.001$). (d) Appressoria formation of different strains on hydrophobic surfaces. Error bars represent standard errors. (e) Cytorrhysis assay for appressoria turgor pressure of different strains. Drops of conidial suspension were placed on the hydrophobic surface of a coverslip and treated with the indicated concentration of glycerine at 24 h post-inoculation (hpi). Error bars represent standard errors, and asterisks represent significant differences (**, $P < 0.01$). (f) Virulence test of different strains on barley leaves. (g) Lesions formed on wounded rice leaves. (h) Observation of different strains infecting host cells. Bar, 25 μm. (i) Conidium, appressorium and infection hyphae formation of different strains at 24 hpi. WT, wild-type strains; Δ*atg8*, *ATG8* deletion mutant; Δ*atg8*/ATG8^{A982C}, *ATG8* complementary strain containing A982C m^{6}A site mutation; Δ*atg8/ATG8*, *ATG8* complementary strain. Error bars represent standard errors.

enhancing role of m^{6}A in mRNA stability of plants, such as MTA- and VIR-mediated m^{6}A modifications (Anderson *et al.*, 2018; Parker *et al.*, 2020). These seemingly contradictory results may be due to different cellular fates or developmental stages, which are mediated by different readers of m6A.

We found that MTA1-mediated m^{6}A modification plays a key role in appressorial autophagy process. We analysed the m^{6}A site in the 3′ UTR region of *MoATG8*, and found that MTA1 regulates the m^{6}A modification of *MoATG8* mRNA at the A982 site, which affects the stability of *ATG8* mRNA. Recently, several other studies also indicated that m^{6}A modification could play roles in regulation of the autophagy process, through regulating mRNA processing of autophagy-related genes (Gulati *et al.*, 2013; Jin *et al.*, 2018; Song *et al.*, 2019; Wang *et al.*, 2020). The m^{6}A demethylase FTO is reported to upregulate the protein abundance of autophagy-related protein kinase ULK1, and is therefore required for autophagy (Jin *et al.*, 2018). Another study in mouse showed that FTO can activate the MTORC1 pathway to regulate the autophagy process (Gulati *et al.*, 2013). The m^{6}A modification is also important for preadipocytes autophagy and adipogenesis, through regulating the expression of *ATG5* and *ATG7* in an m^{6}A-dependent manner (Wang *et al.*, 2020). Taken together, m6A modification may serve as a conserved mechanism for regulating autophagy by maintaining *ATG* gene mRNA equilibrium.

We proposed a model to show that MTA1-mediated m^{6}A plays a key role in regulating autophagy during appressorium

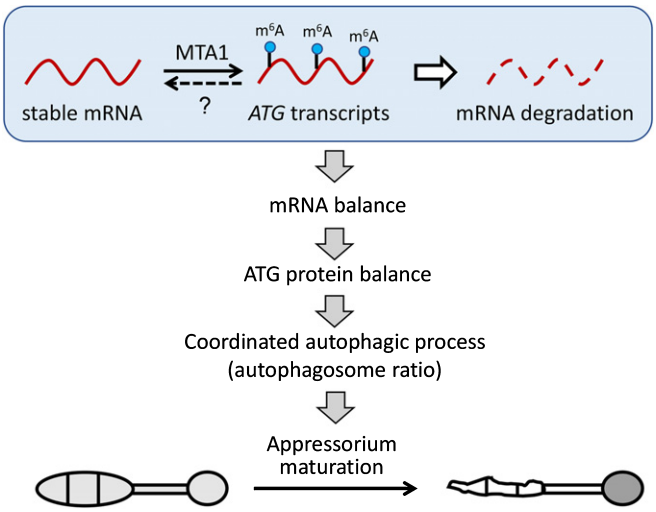

Fig. 10 Working model of the mechanism of MTA1 regulates autophagy in an m^{6}A-dependent manner. In this model, MTA1 regulates the m^{6}A modification of autophagy-related proteins (*ATG*) gene transcripts, which in turn mediate mRNA degradation, therefore the mRNA levels of the *ATG* genes can be well balanced by m^{6}A methylation and de-methylation. This mRNA level balance will contribute to ATG protein balance and, in turn, coordinate the autophagic process (autophagosome ratio), thereby controlling the balance of autophagy in appressoria, and facilitate appressorium maturation and host penetration. Solid black arrows indicate the demonstrated process, and dashed black arrow indicates a predicted process. The interrogation mark means there could be a regulator protein to regulate the predicted de-methylation process.

maturation (Fig. 10). MTA1 mediates the mRNA m^{6}A modification of *ATG* genes, which would lead to degradation of these mRNAs. As a result, the mRNA level of the *ATG* genes will be well balanced by m^{6}A methylation and de-methylation, although the de-methylation enzyme requires confirmation. This mRNA level balance will contribute to the protein level balance, in turn, coordinating the autophagic process, and thereby controls the balance of autophagy in appressorium, and in facilitating appressorium maturation. In the wild-type during appressorium maturation, with the autophagosomes accumulated and degraded in the vacuoles, no new autophagosomes were produced and the autophagy was completed and switched off. Whereas in the Δ*mta1* mutant, new autophagosomes were continuously produced and delivered to the vacuole, the autophagy flow was increased and not switched off. However, the function of the autophagic process may be not so efficient in the Δ*mta1* mutant, because the utilisation of conidial storage during appressorium is defective in the mutant. Our study highlights the functional importance and regulatory mechanism of the m^{6}A in *M. oryzae*. These findings provide insights into the underlying molecular mechanisms of m^{6}A modification in filamentous fungi, which could help us in the development of novel fungicides for fungal disease control.

Acknowledgements

We thank XD, ZL, TL, MQ, ZQ, FL and ZZ for their assistance in additional experiments during the revision process. This work was supported by the National Natural Science Foundation of China (grant nos. 32072365 and 31871909), Fundamental Research Funds for the Central Universities (2021ZKPY007) and the Open Research Fund of the State Key Laboratory of Hybrid Rice (Hunan Hybrid Rice Research Center) (2019KF04).

Author contributions

XLC conceived the project, ZR, CL, XC, AH and MK performed the biological experiments, BT performed the bioinformatic analyses, JX, LZ, HL, JH interpreted results, XLC and BT wrote the paper. ZR and BT contributed equally to this work.

ORCID

Xiao-Lin Chen https://orcid.org/0000-0002-5492-516X
Lu Zheng https://orcid.org/0000-0002-2414-1671

Data availability

All data needed to evaluate the conclusions in the paper are present in the paper and/or the Supporting Information. Raw data of the m6A-seq and RNA-seq were submitted to the sequence read archive (SRA) database with a combined accession no. (PRJNA721132).

References

Aguilo F, Zhang F, Sancho A, Fidalgo M, Di Cecilia S, Vashisht A, Lee D-F, Chen C-H, Rengasamy M, Andino B *et al.* 2015. Coordination of m^{6}A mRNA methylation and gene transcription by ZFP217 regulates pluripotency and reprogramming. *Cell Stem Cell* **17**: 689–704.

Anderson SJ, Kramer MC, Gosai SJ, Yu X, Vandivier LE, Nelson ADL, Anderson ZD, Beilstein MA, Fray RG, Lyons E *et al.* 2018. N^6-methyladenosine inhibits local ribonucleolytic cleavage to stabilize mRNAs in *Arabidopsis*. *Cell Reports* **25**: 1146–1157.

Arribas-Hernández L, Bressendorff S, Hansen MH, Poulsen C, Erdmann S, Brodersen P. 2018. An m^{6}A-YTH module controls developmental timing and morphogenesis in *Arabidopsis*. *Plant Cell* **30**: 952–967.

Batista P, Molinie B, Wang J, Qu K, Zhang J, Li L, Bouley D, Lujan E, Haddad B, Daneshvar K *et al.* 2014. m^{6}A RNA modification controls cell fate transition in mammalian embryonic stem cells. *Cell Stem Cell* **15**: 707–719.

Bento CF, Renna M, Ghislat G, Puri C, Ashkenazi A, Vicinanza M, Menzies FM, Rubinsztein DC. 2016. Mammalian autophagy: how does it work? *Annual Review of Biochemistry* **85**: 685–713.

Chen H, Gu L, Orellana EA, Wang Y, Guo J, Liu QI, Wang L, Shen Z, Wu H, Gregory RI *et al.* 2020. METTL4 is an snRNA m^{6}Am methyltransferase that regulates RNA splicing. *Cell Research* **30**: 544–547.

Clancy MJ, Shambaugh ME, Timpte CS, Bokar JA. 2002. Induction of sporulation in *Saccharomyces cerevisiae* leads to the formation of N^6-methyladenosine in mRNA: a potential mechanism for the activity of the IME4 gene. *Nucleic Acids Research* **30**: 4509–4518.

Deng YZ, Naqvi NI. 2010. A vacuolar glucoamylase, Sga1, participates in glycogen autophagy for proper asexual differentiation in *Magnaporthe oryzae*. *Autophagy* **6**: 455–461.

Deng YZ, Ramos-Pamplona M, Naqvi NI. 2009. Autophagy-assisted glycogen catabolism regulates asexual differentiation in *Magnaporthe oryzae*. *Autophagy* **5**: 33–43.

Duan HC, Wei LH, Zhang C, Wang Y, Chen L, Lu Z, Chen PR, He C, Jia G. 2017. ALKBH10B is an RNA N^6-methyladenosine demethylase affecting Arabidopsis floral transition. *Plant Cell* **29**: 2995–3011.

Fu Y, Dominissini D, Rechavi G, He C. 2014. Gene expression regulation mediated through reversible m^{6}A RNA methylation. *Nature Reviews Genetics* **15**: 293–306.

Füllgrabe J, Ghislat G, Cho DH, Rubinsztein DC. 2016. Transcriptional regulation of mammalian autophagy at a glance. *Journal of Cell Science* **129**: 3059–3066.

Fustin J-M, Doi M, Yamaguchi Y, Hida H, Nishimura S, Yoshida M, Isagawa T, Morioka M, Kakeya H, Manabe I *et al.* 2013. RNA-methylation-dependent RNA processing controls the speed of the circadian clock. *Cell* **155**: 793–806.

Geula S, Moshitch-Moshkovitz S, Dominissini D, Mansour AA, Kol N, Salmon-Divon M, Hershkovitz V, Peer E, Mor N, Manor YS *et al.* 2015. Stem cells. m^{6}A mRNA methylation facilitates resolution of naïve pluripotency toward differentiation. *Science* **347**: 1002–1006.

Goh YT, Koh CWQ, Sim DY, Roca X, Goh WSS. 2020. METTL4 catalyzes m^{6}Am methylation in U2 snRNA to regulate pre-mRNA splicing. *Nucleic Acids Research* **48**: 9250–9261.

Goswami RS. 2012. Targeted gene replacement in fungi using a split-marker approach. *Methods in Molecular Biology* **835**: 255–269.

Gu L, Wang L, Chen H, Hong J, Shen Z, Dhall A, Lao T, Liu C, Wang Z, Xu Y *et al.* 2020. CG14906 (mettl4) mediates m^{6}A methylation of U2 snRNA in *Drosophila*. *Cell Discovery* **6**: 44.

Gulati P, Cheung MK, Antrobus R, Church CD, Harding HP, Tung YC, Rimmington D, Ma M, Ron D, Lehner PJ *et al.* 2013. Role for the obesity-related FTO gene in the cellular sensing of amino acids. *Proceedings of the National Academy of Sciences, USA* **110**: 2557–2562.

Hao Z, Wu T, Cui X, Zhu P, Tan C, Dou X, Hsu K-W, Lin Y-T, Peng P-H, Zhang L-S *et al.* 2020. N^6-deoxyadenosine methylation in mammalian mitochondrial DNA. *Molecular Cell* **78**: 382–395.

He M, Kershaw MJ, Soanes DM, Xia Y, Talbot NJ. 2012. Infection-associated nuclear degeneration in the rice blast fungus *Magnaporthe oryzae* requires non-selective macro-autophagy. *PLoS ONE* **7**: e33270.

He M, Xu Y, Chen J, Luo Y, Lv Y, Su J, Kershaw MJ, Li W, Wang J, Yin J *et al.* 2018. MoSnt2-dependent deacetylation of histone H3 mediates MoTor-dependent autophagy and plant infection by the rice blast fungus *Magnaporthe oryzae*. *Autophagy* **14**: 1543–1561.

He PC, He C. 2021. m^{6}A RNA methylation: from mechanisms to therapeutic potential. *EMBO Journal* **40**: e105977.

Ivanova I, Much C, Di Giacomo M, Azzi C, Morgan M, Moreira PN, Monahan J, Carrieri C, Enright AJ, O'Carroll D. 2017. The RNA m^{6}A reader YTHDF2 is essential for the post-transcriptional regulation of the maternal transcriptome and oocyte competence. *Molecular Cell* **67**: 1059–1067.

Jia G, Fu YE, Zhao XU, Dai Q, Zheng G, Yang Y, Yi C, Lindahl T, Pan T, Yang Y-G *et al.* 2011. N^6-methyladenosine in nuclear RNA is a major substrate of the obesity-associated FTO. *Nature Chemical Biology* **7**: 885–887.

Jin S, Zhang X, Miao Y, Liang P, Zhu K, She Y, Wu Y, Liu D-A, Huang J, Ren J *et al.* 2018. m^{6}A RNA modification controls autophagy through upregulating ULK1 protein abundance. *Cell Research* **28**: 955–957.

Kan L, Grozhik AV, Vedanayagam J, Patil DP, Pang N, Lim K-S, Huang Y-C, Joseph B, Lin C-J, Despic V *et al.* 2017. The m^{6}A pathway facilitates sex determination in *Drosophila*. *Nature Communications* **8**: 15737.

Kershaw MJ, Talbot NJ. 2009. Genome-wide functional analysis reveals that infection-associated fungal autophagy is necessary for rice blast disease. *Proceedings of the National Academy of Sciences, USA* **106**: 15967–15972.

Kweon SM, Chen Y, Moon E, Kvederaviciutė K, Klimasauskas S, Feldman DE. 2019. An adversarial DNA N^6-methyladenine-sensor network preserves polycomb silencing. *Molecular Cell* **74**: 1138–1147.

Lence T, Akhtar J, Bayer M, Schmid K, Spindler L, Ho CH, Kreim N, Andrade-Navarro MA, Poeck B, Helm M *et al.* 2016. m^{6}A modulates neuronal functions and sex determination in *Drosophila*. *Nature* **540**: 242–247.

Lin S, Choe J, Du P, Triboulet R, Gregory RI. 2016. The m^{6}A methyltransferase METTL3 promotes translation in human cancer cells. *Molecular Cell* **62**: 335–345.

Liu J, Yue Y, Han D, Wang X, Fu Y, Zhang L, Jia G, Yu M, Lu Z, Deng X *et al.* 2014. A METTL3-METTL14 complex mediates mammalian nuclear RNA N^6-adenosine methylation. *Nature Chemical Biology* **10**: 93–95.

Liu N, Dai Q, Zheng G, He C, Parisien M, Pan T. 2015. *N*^{6}-methyladenosine-dependent RNA structural switches regulate RNA-protein interactions. *Nature* **518**: 560–564.

Liu XH, Gao HM, Xu F, Lu JP, Devenish RJ, Lin FC. 2012. Autophagy vitalizes the pathogenicity of pathogenic fungi. *Autophagy* **8**: 1415–1425.

Ma H, Wang X, Cai J, Dai Q, Natchiar SK, Lv R, Chen K, Lu Z, Chen H, Shi YG *et al.* 2019. *N*^{6}-methyladenosine methyltransferase ZCCHC4 mediates ribosomal RNA methylation. *Nature Chemical Biology* **15**: 88–94.

Marroquin-Guzman M, Sun G, Wilson RA. 2017. Glucose-ABL1-TOR signaling modulates cell cycle tuning to control terminal appressorial cell differentiation. *PLoS Genetics* **13**: e1006557.

Marroquin-Guzman M, Wilson RA. 2015. GATA-dependent glutaminolysis, drives appressorium formation in *Magnaporthe oryzae* by suppressing TOR inhibition of cAMP/PKA signaling. *PLoS Path* **11**: e1004851.

Meyer KD, Patil DP, Zhou J, Zinoviev A, Skabkin MA, Elemento O, Pestova TV, Qian SB, Jaffrey SR. 2015. 5′UTR m^{6}A promotes cap-independent translation. *Cell* **163**: 999–1010.

Motorin Y, Helm M. 2011. RNA nucleotide methylation. *Wiley Interdisciplinary Reviews RNA* **2**: 611–631.

Ohsumi Y. 2014. Historical landmarks of autophagy research. *Cell Research* **24**: 9–23.

Parker MT, Knop K, Sherwood AV, Schurch NJ, Mackinnon K, Gould PD, Hall AJ, Barton GJ, Simpson GG. 2020. Nanopore direct RNA sequencing maps the complexity of Arabidopsis mRNA processing and m^{6}A modification. *eLife* **9**: e49658.

Pendleton KE, Chen B, Liu K, Hunter OV, Xie Y, Tu BP, Conrad NK. 2017. The U6 snRNA m^{6}A methyltransferase METTL16 regulates SAM synthetase intron retention. *Cell* **169**: 824–835.

Ping X-L, Sun B-F, Wang LU, Xiao W, Yang X, Wang W-J, Adhikari S, Shi Y, Lv Y, Chen Y-S *et al.* 2014. Mammalian WTAP is a regulatory subunit of the RNA N^6-methyladenosine methyltransferase. *Cell Research* **24**: 177–189.

Schwartz S, Mumbach M, Jovanovic M, Wang T, Maciag K, Bushkin G, Mertins P, Ter-Ovanesyan D, Habib N, Cacchiarelli D *et al.* 2014. Perturbation of m^{6}A writers reveals two distinct classes of mRNA methylation at internal and 5′ sites. *Cell Reports* **8**: 284–296.

Shen L, Liang Z, Gu X, Chen Y, Teo ZW, Hou X, Cai WM, Dedon PC, Liu L, Yu H. 2016. N^6-methyladenosine RNA modification regulates shoot stem cell fate in *Arabidopsis*. *Developmental Cell* **38**: 186–200.

Shi Y, Wang H, Wang J, Liu X, Lin F, Lu J. 2019. N^6-methyladenosine RNA methylation is involved in virulence of the rice blast fungus *Pyricularia oryzae* (syn. *Magnaporthe oryzae*). *FEMS Microbiology Letters* **366**: 10.

Shibutani ST, Saitoh T, Nowag H, Münz C, Yoshimori T. 2015. Autophagy and autophagy-related proteins in the immune system. *Nature Immunology* **16**: 1014–1024.

Song H, Feng X, Zhang H, Luo Y, Huang J, Lin M, Jin J, Ding X, Wu S, Huang H *et al.* 2019. METTL3 and ALKBH5 oppositely regulate m^{6}A modification of TFEB mRNA, which dictates the fate of hypoxia/reoxygenation-treated cardiomyocytes. *Autophagy* **15**: 1419–1437.

van Tran N, Ernst FGM, Hawley BR, Zorbas C, Ulryck N, Hackert P, Bohnsack KE, Bohnsack MT, Jaffrey SR, Graille M *et al.* 2019. The human 18S rRNA m^{6}A methyltransferase METTL5 is stabilized by TRMT112. *Nucleic Acids Research* **47**: 7719–7733.

Veneault-Fourrey C, Barooah M, Egan M, Wakley G, Talbot NJ. 2006. Autophagic fungal cell death is necessary for infection by the rice blast fungus. *Science* **312**: 580–583.

Visvanathan A, Patil V, Arora A, Hegde AS, Arivazhagan A, Santosh V, Somasundaram K. 2018. Essential role of METTL3-mediated m^{6}A modification in glioma stem-like cells maintenance and radio resistance. *Oncogene* **37**: 522–533.

Wang P, Doxtader KA, Nam Y. 2016. Structural basis for cooperative function of Mettl3 and Mettl14 methyltransferases. *Molecular Cell* **63**: 306–317.

Wang X, Lu Z, Gomez A, Hon GC, Yue Y, Han D, Fu YE, Parisien M, Dai Q, Jia G *et al.* 2014. N^6-methyladenosine-dependent regulation of messenger RNA stability. *Nature* **505**: 117–120.

Wang X, Wu R, Liu Y, Zhao Y, Bi Z, Yao Y, Liu Q, Shi H, Wang F, Wang Y. 2020. m^6A mRNA methylation controls autophagy and adipogenesis by targeting Atg5 and Atg7. *Autophagy* **16**: 1221–1235.

Wang X, Zhao BS, Roundtree IA, Lu Z, Han D, Ma H, Weng X, Chen K, Shi H, He C. 2015. N^6-methyladenosine modulates messenger RNA translation efficiency. *Cell* **161**: 1388–1399.

Wani WY, Boyer-Guittaut M, Dodson M, Chatham J, Darley-Usmar V, Zhang J. 2015. Regulation of autophagy by protein post-translational modification. *Laboratory Investigation* **95**: 14–25.

Warda AS, Kretschmer J, Hackert P, Lenz C, Urlaub H, Höbartner C, Sloan KE, Bohnsack MT. 2017. Human METTL16 is a N^6-methyladenosine (m^6A) methyltransferase that targets pre-mRNAs and various non-coding RNAs. *EMBO Reports* **18**: 2004–2014.

Wei LH, Song P, Wang Y, Lu Z, Tang Q, Yu Q, Xiao Y, Zhang X, Duan HC, Jia G. 2018. The m^6A reader ECT2 controls trichome morphology by affecting mRNA stability in *Arabidopsis*. *Plant Cell* **30**: 968–985.

Wen J, Lv R, Ma H, Shen H, He C, Wang J, Jiao F, Liu H, Yang P, Tan LI *et al.* 2018. Zc3h13 regulates nuclear RNA m^6A methylation and mouse embryonic stem cell self-renewal. *Molecular Cell* **69**: 1028–1038.e6.

Wilson RA, Talbot NJ. 2009. Under pressure: investigating the biology of plant infection by *Magnaporthe oryzae*. *Nature Reviews Microbiology* **7**: 185–195.

Yadav PK, Rajasekharan R. 2017. The m^6A methyltransferase Ime4 epitranscriptionally regulates triacylglycerol metabolism and vacuolar morphology in haploid yeast cells. *Journal of Biological Chemistry* **292**: 13727–13744.

Yadav PK, Rajasekharan R. 2018. The m^6A methyltransferase Ime4 and mitochondrial functions in yeast. *Current Genetics* **64**: 353–357.

Yin Z, Chen C, Yang J, Feng W, Liu X, Zuo R, Wang J, Yang L, Zhong K, Gao C *et al.* 2019. Histone acetyltransferase MoHat1 acetylates autophagy-related proteins MoAtg3 and MoAtg9 to orchestrate functional appressorium formation and pathogenicity in *Magnaporthe oryzae*. *Autophagy* **15**: 1234–1257.

Yu L, Chen Y, Tooze SA. 2018. Autophagy pathway: cellular and molecular mechanisms. *Autophagy* **14**: 207–215.

Yue Y, Liu J, Cui X, Cao J, Luo G, Zhang Z, Cheng T, Gao M, Shu X, Ma H *et al.* 2018. VIRMA mediates preferential m^6A mRNA methylation in 3′UTR and near stop codon and associates with alternative polyadenylation. *Cell Discovery* **4**: 10.

Zhao BS, Wang X, Beadell AV, Lu Z, Shi H, Kuuspalu A, Ho RK, He C. 2017. m^6A-dependent maternal mRNA clearance facilitates zebrafish maternal-to-zygotic transition. *Nature* **542**: 475–478.

Zheng G, Dahl J, Niu Y, Fedorcsak P, Huang C-M, Li C, Vågbø C, Shi Y, Wang W-L, Song S-H *et al.* 2013. ALKBH5 is a mammalian RNA demethylase that impacts RNA metabolism and mouse fertility. *Molecular Cell* **49**: 18–29.

Zhou L, Tian S, Qin G. 2019. RNA methylomes reveal the m^6A-mediated regulation of DNA demethylase gene SlDML2 in tomato fruit ripening. *Genome Biology* **20**: 156.

Zhu XM, Li L, Wu M, Liang S, Shi HB, Liu XH, Lin FC. 2019. Current opinions on autophagy in pathogenicity of fungi. *Virulence* **10**: 481–489.

Supporting Information

Additional Supporting Information may be found online in the Supporting Information section at the end of the article.

Fig. S1 Deletion of *MTA1* in *Magnaporthe oryzae* and verification of the transformants.

Fig. S2 Expression of *MTA1* gene during different development and infection stages of *Magnaporthe oryzae*.

Fig. S3 *MTA1* disruption affects vegetative growth of *Magnaporthe oryzae*.

Fig. S4 The deletion mutant of *MTA1* is sensitive to different stresses.

Fig. S5 *Magnaporthe oryzae* Δ*mta1* mutant stimulates host immune responses.

Fig. S6 m^6A sequencing using appressorium of wild-type and the Δ*mta1* mutant at 12 hpi.

Table S1 Fungal strains used in this study.

Table S2 Plasmids used in this study.

Table S3 All m6A peaks of transcripts identified by m6A-seq.

Table S4 All gene expression patterns identified by RNA-seq.

Table S5 Differentially expressed genes in the Δ*mta1* mutants.

Table S6 m6A-seq results for transcripts of the autophagy-related genes.

Please note: Wiley Blackwell are not responsible for the content or functionality of any Supporting Information supplied by the authors. Any queries (other than missing material) should be directed to the *New Phytologist* Central Office.